MOLECULAR
METABOLISM

Adult-born proopiomelanocortin neurons derived from *Rax*-expressing precursors mitigate the metabolic effects of congenital hypothalamic proopiomelanocortin deficiency

Surbhi [1,3], Gábor Wittmann [2,3], Malcolm J. Low [1], Ronald M. Lechan [2,*]

ABSTRACT

Objective: Proopiomelanocortin (POMC) neurons of the hypothalamic arcuate nucleus are essential regulators of energy balance. Selective loss of POMC production in these cells results in extreme obesity and metabolic comorbidities. Neurogenesis occurs in the adult hypothalamus, but it remains uncertain whether functional POMC neurons emerge in physiologically significant numbers during adulthood. Here, we tested whether *Rax*-expressing precursors generate POMC neurons in adult mice and rescue the metabolic phenotype caused by congenital hypothalamic POMC deficiency.

Methods: Initially, we identified hypothalamic *Rax*-expressing cell types using wild-type and *Rax-CreERT2:Ai34D* mice. Then we generated compound *Rax-CreERT2*:Arc*Pomc*$^{loxTB/loxTB}$ mice in which endogenous hypothalamic *Pomc* expression is silenced, but can be restored by tamoxifen administration selectively in neurons derived from *Rax*$^+$ progenitors. The number of POMC neurons generated by *Rax*$^+$ progenitors in adult mice and their axonal projections was determined. The metabolic effects of these neurons were assessed by measuring food intake, bodyweight, and body composition, along with glucose and insulin levels.

Results: We found that *Rax* is expressed by tanycytes and a previously unrecognized cell type in the hypothalamic parenchyma of adult mice. *Rax*$^+$ progenitors generated ~10% of the normal adult hypothalamic POMC neuron population within two weeks of tamoxifen treatment. The same rate and steady state of POMC neurogenesis persisted from young adult to aged mice. These new POMC neurons established terminal projections to brain regions that were involved in energy homeostasis. Mice with *Rax*$^+$ progenitor-derived POMC neurons had reduced body fat mass, improved glucose tolerance, increased insulin sensitivity, and decreased bodyweight in proportion to the number of new POMC neurons.

Conclusions: These data demonstrate that *Rax*$^+$ progenitors generate POMC neurons in sufficient numbers during adulthood to mitigate the metabolic abnormalities of hypothalamic POMC-deficient mice. The findings suggest that adult hypothalamic neurogenesis is a robust phenomenon in mice that can significantly impact energy homeostasis.

Keywords POMC; *Rax*; Adult neurogenesis; Tanycyte; Stem cell; Arcuate nucleus

1. INTRODUCTION

Obesity and type 2 diabetes have emerged as a global health crisis in recent decades. Bodyweight and energy balance are regulated by multiple interacting neural circuits in the brain [1], an essential component of which is the melanocortin system in both rodents and humans [2]. Proopiomelanocortin (POMC) neurons in the hypothalamic arcuate nucleus (Arc) inhibit food intake and stimulate energy expenditure by releasing α-melanocyte-stimulating hormone (α-MSH), which further stimulates downstream satiety neurons expressing melanocortin receptors [3]. Mice with a selective deletion of *Pomc* expression in Arc neurons develop a severely obese phenotype characterized by hyperphagia, hyperinsulinemia, and reduced energy expenditure [4,5]. Using a reversible genetic mouse model of Arc *Pomc* deficiency, we previously demonstrated that the restoration of eutopic *Pomc* expression in Arc neurons of weanling mice resulted in the complete rescue of the obese phenotype [5]. Reactivation of Arc *Pomc* expression in adult mice with increased levels of overweight — while not completely normalizing bodyweight or leptin sensitivity — markedly reduced the level of obesity and associated comorbidities [5]. However,

[1]Department of Molecular & Integrative Physiology, University of Michigan Medical School, 2800 Plymouth Rd, Ann Arbor, MI, 48109, USA [2]Department of Medicine, Division of Endocrinology, Diabetes and Metabolism, Tufts Medical Center, 800 Washington St, Boston, MA, 02111, USA

[3] Surbhi and Gábor Wittmann contributed equally to this work.

*Corresponding author. Department of Medicine, Division of Endocrinology, Diabetes, and Metabolism, Tufts Medical Center, Box #268, 800 Washington Street, Boston, MA, 02111, USA.

E-mails: sgahlot@umich.edu (Surbhi), gabor.wittmann11@gmail.com (G. Wittmann), mjlow@umich.edu (M.J. Low), rlechan@tuftsmedicalcenter.org (R.M. Lechan).

Original Article

Abbreviations

			IF	immunofluorescence
			loxTB	*loxP*-flanked transcription blocker sequence
α-MSH	α-melanocyte-stimulating hormone		MCT8	monocarboxylate transporter 8
Arc	arcuate nucleus		NTS	nucleus of the solitary tract
ANOVA	analysis of variance		POA	preoptic area
AUC	area under the curve		POMC	proopiomelanocortin
BNST	bed nucleus of the stria terminalis		PVH	paraventricular hypothalamic nucleus
BrdU	bromodeoxyuridine		TAM	tamoxifen
DMH	dorsomedial hypothalamic nucleus		tdTom	tdTomato
FISH	fluorescence *in situ* hybridization		VMH	ventromedial hypothalamic nucleus
GFAP	glial fibrillary acidic protein		WT	wild-type
GTT	glucose tolerance test			

chronic food restriction to normalize bodyweight before the reactivation of Arc *Pomc* expression restored leptin sensitivity and resulted in the indefinite maintenance of normal bodyweight and body composition [6].

Considering the efficacy of *Pomc* expression rescue, and recent evidence of adult hypothalamic neurogenesis in mammals [7], promoting *Pomc* neurogenesis postnatally could lead to a new treatment for obesity and associated metabolic comorbidities in humans. However, it remains uncertain whether functional *Pomc* neurons emerge normally during adulthood and reach a critical mass that can favorably impact energy homeostasis. Studies that applied brain delivery of the cell proliferation marker, bromodeoxyuridine (BrdU), detected only a small number of Arc *Pomc* neurons that derived from new cell divisions in adult mice [8,9]. Somewhat more, albeit still a low number of adult-born *Pomc* neurons, were identified by fate mapping of *Sox2*-expressing neural progenitors of the mediobasal hypothalamic parenchyma in adult mice [8]. However, an indirect approach based on tracking the survival rate of prenatally generated POMC neurons into adulthood suggested that a stunning 50% of Arc POMC neurons might be replaced by ongoing neurogenesis between 4 and 12 weeks of age in mice [10].

Besides parenchymal progenitors, another population of adult hypothalamic stem/progenitor cells is tanycytes — radial glia-like ependymal cells lining the third ventricle — that can differentiate into glia and neurons [11—15]. While tanycytes were recently shown to give rise to some POMC neurons in the early postnatal period (postnatal day 8) [16], the capacity of tanycytes to generate functionally relevant POMC neurons during adulthood is unknown. The present study was designed to systematically test whether tanycytes can differentiate into melanocortin-secreting POMC neurons that integrate into the normal anatomical projection pathways, and rescue the obesity phenotype caused by the loss of *Pomc* expression in Arc *Pomc*-deficient mice. We generated an inducible compound genetic mouse model by crossing Arc*Pomc*^loxTB/loxTB^ mice with reversible *Pomc* silencing in the Arc [5] with *Rax-CreERT2* knock-in mice [17] expressing tamoxifen (TAM)-inducible CreERT2 under the endogenous *Rax* promoter/enhancers, the most selective marker known for tanycytes [17—20]. TAM treatment of these mice induces Cre recombinase activity that matches the endogenous *Rax* expression pattern and relieves the transcriptional silencing of *Pomc* in *Rax*-positive cells—thus allowing *Pomc* transcriptional activity only in neurons derived from *Rax*+ progenitors. Using this model, we aimed to dissect the role of *Rax*+ progenitors in the generation of hypothalamic POMC neurons in young adult to aged mice, and to decipher the capacity of these new neurons to restore the metabolic abnormalities observed in Arc *Pomc*-deficient mice.

2. MATERIALS AND METHODS

2.1. Animal care
All animal procedures were approved by the Institutional Animal Care and Use Committees at the University of Michigan and Tufts Medical Center, and followed the National Research Council's "Guide for the Care and Use of Laboratory Animals". Mice were group-housed (3—5 per cage) on cellulose bedding in ventilated cages under controlled temperature (25 ± 4 °C) and photoperiod (12-h light—dark cycle, lights on from 6:00 am to 6:00 pm), with filtered tap water and standard laboratory chow (5LOD; LabDiet, St. Louis, MO) that contained 28.5 kcal% protein, 13.5 kcal% fat, and 58.0 kcal% carbohydrate available *ad libitum*. All breeders were fed *ad libitum* with breeder chow (5008; LabDiet) that contained 26.53 kcal% protein, 16.97 kcal% fat, and 56.5 kcal% carbohydrate. For fasting-refeeding and metabolic experiments, mice were individually housed and either fed *ad libitum* or preweighed amount of food, or were fasted overnight by removing the chow diet from the cages depending on the purpose of the experiments and according to the approved experimental protocol.

2.2. Generation and breeding of mice
Arc*Pomc*^loxTB/loxTB^ mice were generated on the C57BL/6J background as described with the alternate name Arc*Pomc*^−/−^ [5,21]. Arc*Pomc*^loxTB/loxTB^ mice carry a *loxP*-flanked transcription blocker sequence (*loxTB*; a pGK-*neo* cassette), inserted between the first upstream neuronal enhancer (nPE1) and the deleted second neuronal enhancer (nPE2) of the *Pomc* gene (Figure 1A). The presence of *loxTB* in the neuronal enhancer region selectively blocks *Pomc* gene expression in neurons of the hypothalamic arcuate nucleus, while expression in the pituitary and nucleus of the solitary tract (NTS) remains intact [21] (Figure 1A). Arc*Pomc*^loxTB/loxTB^ mice are obese and hyperphagic due to the lack of *Pomc* gene expression in the Arc, which can be rescued by TAM-induced CreERT2-mediated removal of *loxTB* [5].

Arc*Pomc*^loxTB/loxTB^ mice were crossed with *Rax-CreERT2* knock-in mice (*Rax*^tm1.1(cre/ERT2)Sbls^/J; The Jackson Laboratory) to obtain compound *Rax-CreERT2/+*:Arc*Pomc*^loxTB/loxTB^ mice (Figure 1A). *Rax-CreERT2/+* transgenic mice were generated on the C57BL/6J background and express TAM-inducible Cre recombinase activity under the direction of the *Rax* promoter and enhancers [17].

The inducible triple compound *Rax-CreERT2/+*:Arc*Pomc*^loxTB/loxTB^:*Ai34*(RCL-Syp/tdT)-D genetic model was generated by crossing *Rax-CreERT2/+*:Arc*Pomc*^loxTB/loxTB^ mice with *Ai34*(RCL-Syp/tdT)-D mice (B6; 129S-*Gt*(ROSA)26Sor^tm34.1(CAG-Syp/tdTomato)Hze^/J; The Jackson Laboratory). *Ai34D* mice carry a knock-in mutation at the *Gt*(ROSA)26Sor locus with a *loxP*-flanked STOP cassette that prevents the
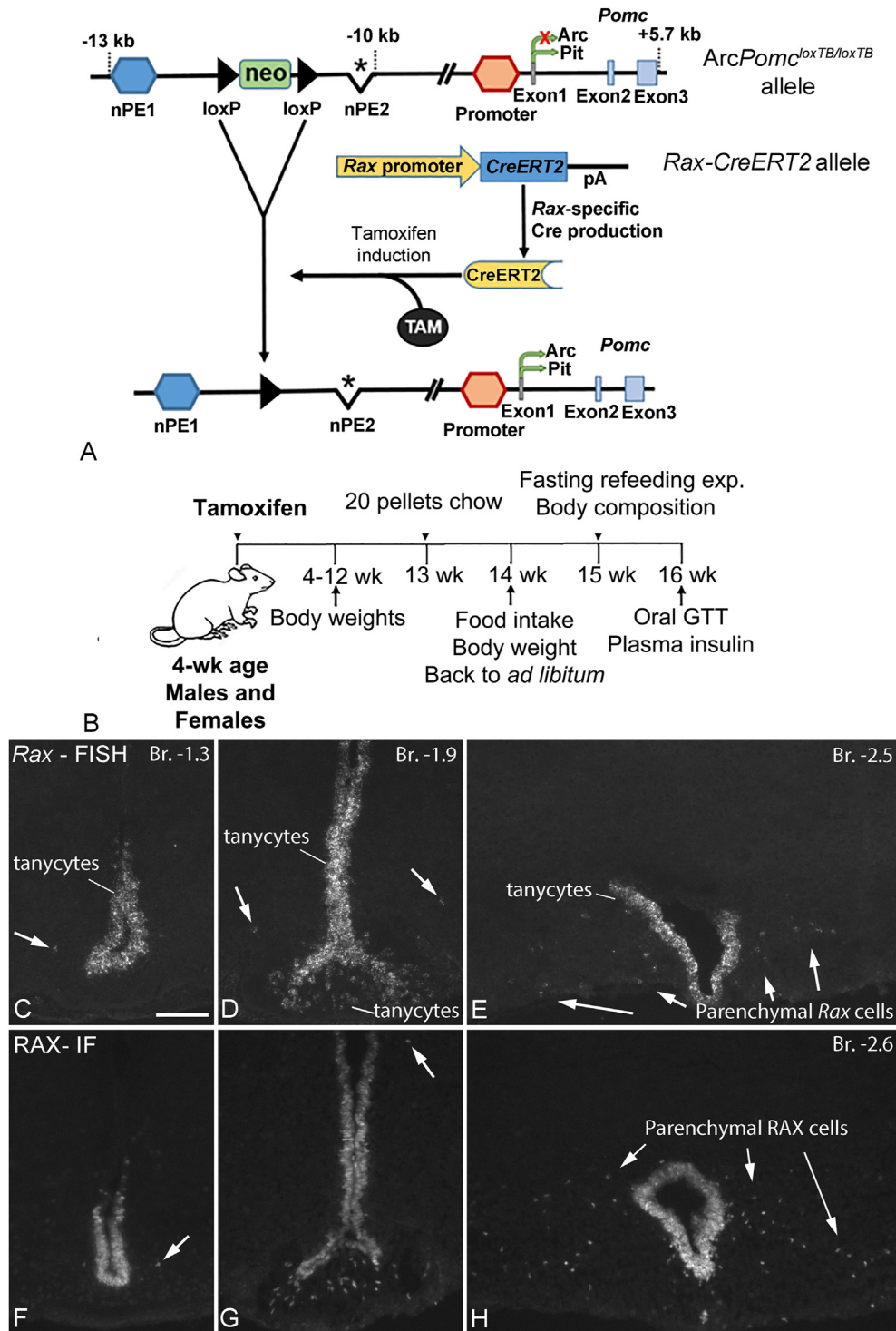
Figure 1: Generation of *Rax-CreERT2/+:ArcPomc^{loxTB/loxTB}* mice, experimental design, and cellular distribution of *Rax* mRNA/RAX protein in the mouse hypothalamus.
(A) ArcPomc^{loxTB/loxTB} mice carry a floxed transcription blocker (neo cassette) in the neuronal enhancer region of the *Pomc* gene that prevents *Pomc* transcription in Arc neurons, but not the pituitary. When *Rax*-specific CreERT2 knock-in mice are crossed to ArcPomc^{loxTB/loxTB} mice, the transcription blocker is excised in *Rax*+ cells in response to TAM induction, allowing *Pomc* gene expression in Arc neurons derived from *Rax*+ precursors. **(B)** Timeline and experimental design of the metabolic study. Male and female mice were injected with TAM at age 4−5 weeks, followed by food intake and bodyweight measurements for an additional 16 weeks. Body composition measurements were taken at age 15 weeks and an oral glucose tolerance test (GTT) with insulin measurements were performed at age 16 weeks. **(C−E)** FISH shows the distribution of *Rax* mRNA-expressing cells at different rostrocaudal levels (Bregma coordinates are indicated). *Rax* is expressed in tanycytes lining the 3rd ventricle, in the median eminence, and in parenchymal cells (arrows) that constitute a small but significant cell population in the caudal Arc. **(F−H)** Immunofluorescence (IF) for RAX (transcription factor protein encoded by *Rax*), labels cell nuclei in the same distribution pattern as *Rax* mRNA. Scale bar: 100 μm **(C,** for **C−H)**.

Original Article

transcription of a CAG (cytomegalovirus early enhancer element; the promoter, the first exon and the first intron of the chicken beta-Actin gene; and the splice acceptor of the rabbit beta-Globin) promoter-driven *synaptophysin-tdTomato* fusion gene. Cre-mediated removal of the STOP cassette results in synaptophysin-tdTomato expression in neuronal soma, projections, and synaptic terminals in brain regions.

2.3. Genotyping

Mouse genotyping was performed by extracting the DNA from tail tips; it was collected carefully with fresh razor blades to avoid cross-contamination between the samples. Tails were incubated at 55 °C overnight in a lysis solution that contained proteinase K (0.1 μg/μl). DNA extraction was performed as described previously [22].

After the compound *Rax-CreERT2/+:ArcPomc$^{loxTB/loxTB}$:Ai34(RCL-Syp/tdT)-D* transgenic line was established, the presence of the *Rax-CreERT2* allele was determined by polymerase chain reaction (PCR) using primers amplifying the *Cre* recombinase: forward 5′-GGA-CATGTTCAGGGATCGCCAGGCG-3′ and reverse 5′-GCATAACCAGTG AAACAGCATTGCTG-3′, which produced a 268 bp PCR product. Genotyping for Arc*Pomc$^{loxTB/loxTB}$* was performed using primers: forward 5′-GGGTGGGCTACTGTGCTAATA-3′ and reverse 5′-AAGCCAAGAGCA-CACTGAAGGAGA -3′, which produced a 178 bp band for the *loxTB* knock-in allele and 346 bp band for the wild-type (WT) allele. *Ai34(RCL-Syp/tdT)-D* mice were genotyped by using the forward primer 5′-GGAGTGTGCCAACAAGACGGAGA-3′ and reverse primer 5′-CCAGCCTGTCTCCTTGAACACGA-3′, which produced a 523 bp band for the transgenic allele and 297 bp band for the WT allele. The PCR protocol used was as follows: 94 °C for 4 min, followed by 35 cycles of 94 °C for 1 min, 67 °C for 1 min, 72 °C for 1 min, 72 °C for 5 min, and 4 °C on hold.

2.4. General experimental design

Experiment 1. *Rax mRNA and RAX protein expression study in WT mice.* Juvenile male and female (n = 4 each) C57BL/6NTac mice were purchased from Taconic Farms (Germantown, NY) and euthanized on postnatal day 33.

Experiment 2. *Metabolic study in early adult mice.* Ten cohorts of mice each containing multiple genotypes of mice were generated by using the above breeding strategies. After the genotypes were known, males (WT, n = 9; *Rax-CreERT2/+*, n = 6; Arc*Pomc$^{loxTB/loxTB}$*, n = 6; *Rax-CreERT2/+:ArcPomc$^{loxTB/loxTB}$*, n = 8) and females (WT, n = 3; *Rax-CreERT2/+*, n = 6; Arc*Pomc$^{loxTB/loxTB}$*, n = 8; *Rax-CreERT2/+:ArcPomc$^{loxTB/loxTB}$*, n = 6) at age 4—5 weeks were injected intraperitoneally with TAM (100 mg/kg dose; T5648, Sigma—Aldrich, dissolved in sesame oil, S3547, Sigma—Aldrich) for five consecutive days [23]. Some of these mice also carried the *Ai34D* allele; refer Results section 3.7. Following TAM treatment, mice were monitored for serial bodyweight, food intake, whole body composition (fat mass, lean mass, and fluid mass), oral glucose tolerance test (GTT), and insulin measurements for 16 additional weeks (Figure 1B) [24].

Experiment 3. *Age cohort study.* Eight cohorts of mice, from 15 to 50 weeks old, were injected with TAM as described and monitored weekly for bodyweight for 12—16 weeks, and then, euthanized. In total, this experiment included 4 male and 6 female *Rax-CreERT2/+*; 5 male and 3 female Arc*Pomc$^{loxTB/loxTB}$*; and 14 male and 12 female *Rax-CreERT2/+:ArcPomc$^{loxTB/loxTB}$* mice. The exact ages of the mice are described in Results section 3.5 and Figure 7.

Experiment 4. *Short-term survival study.* Mice were injected with TAM and euthanized 7 days or 16 days after the first of five daily TAM injections. For the histologic analysis, the 7-day group included 3 male and 5 female *Rax-CreERT2/+:ArcPomc$^{loxTB/loxTB}$* mice (some carrying the *Ai34D* allele, refer Results section 3.7), 1 male and 1 female Arc*Pomc$^{loxTB/loxTB}$* mice, and 1 male and 2 female *Rax-CreERT2/+:Ai34D* mice. The 16-day group included 3 male and 1 female *Rax-CreERT2/+:ArcPomc$^{loxTB/loxTB}$* mice and 3 male Arc*Pomc$^{loxTB/loxTB}$* mice. The age of the mice is described in Figure 8 and Supplementary Fig. 5.

2.5. Bodyweight and food intake measurements

After TAM treatment, both male and female mice were subjected to bodyweight measurements that started at the age of 4—5 weeks. At 12 weeks' age, mice were acclimated to single housing with standard laboratory chow and filtered tap water *ad libitum* for one week. After one-week acclimation, at 13 weeks' age, mice were weighed to ensure the recovery of their bodyweights after changes in the housing conditions. Mice were then transferred to clean cages and provided with preweighed food (20 chow pellets = ~80—100 g per mouse). After one week, at 14 weeks' age, the mice were weighed and the remaining food was measured to determine average daily food consumption. Mice were then given *ad libitum* food for the remaining week. At 15 weeks' age, the body composition measurements were obtained by nuclear magnetic resonance (NMR), followed by a fasting-refeeding experiment that started at 4 pm on the same day. In this experiment, mice were given preweighed food (6 chow pellets = ~20—25 g per mouse) and food intake was measured daily. After 48 h, mice were weighed and fasted for 18 h. After an 18 h fast, they were again weighed and provided with 3 chow pellets of food. The food intake was measured at 1, 2, 4, and 24 h after the food was given. Mice were weighed after refeeding and fed *ad libitum* over the weekend. At 16 weeks' age, an oral GTT was performed after a 5 h fast. After two days, mice were euthanized by transcardial perfusion as described below.

2.6. Body composition measurements

Body composition measurements were performed by the University of Michigan Animal Phenotyping Core. Body fat, lean mass, and free fluids were measured in live mice using an NMR-based analyzer (Minispec LF90II, Bruker Optics). The noninvasive individual measurements took less than 2 min during which conscious mice were placed into the measuring tube with minimal restraint. Before use, the machine performance was checked daily using a reference sample (canola seeds), as recommended by the manufacturer.

2.7. Oral GTT and insulin measurements

Oral GTT with insulin measurements were performed by the University of Michigan Animal Phenotyping Core. Mice were fasted for 5 h (8 am—1 pm) before the oral administration of 2 g/kg bodyweight glucose (50% glucose in 1X PBS) using 18-gauge oral gavage needles (FNS-18-2; Kent Scientific Corporation). Blood samples were collected through tail vein blood before and after the glucose gavage at 0, 15, 30, 60, and 120 min and were assayed for blood glucose using a glucometer (Acucheck, Roche) and plasma insulin levels using an ELISA kit (#90080, Crystal Chem Ultra-Sensitive Mouse Insulin ELISA Kit, IL, USA). Animals were restrained repeatedly for less than a minute to collect blood samples. The total area under the curve (AUC) for glucose and insulin was calculated using the trapezoidal rule [25]. The glucose-insulin index, an indicator of insulin resistance, was calculated

as the product of the AUC for glucose and insulin [26]. HOMA-IR index, as a homeostatic model assessment of β-cell function and insulin resistance, was calculated as the product of fasting glucose and insulin [27].

2.8. Tissue collection

Mice from Experiment 1 and the 16-day group in Experiment 4 were deeply anesthetized with ketamine/xylazine or isoflurane (Piramal Enterprises Ltd.), respectively, and decapitated. The brains were removed from the skulls and either rapidly immersed in dry ice-chilled isopentane or snap-frozen in powdered dry ice, respectively. Mice from Experiments 2, 3, and 4 (7-day group) were deeply anesthetized with isoflurane and transcardially perfused with 50 ml 0.1 M RNase-free PBS (pH 7.4), followed by 50 ml 4% paraformaldehyde (PFA) in PBS. Brains were dissected out, postfixed overnight in 4% PFA, and then cryoprotected in 30% sucrose (Fisher Scientific) in RNase-free PBS at 4 °C, till the brain tissues sank. All dissections were carried out at mid-day.

Coronal sections were cut through the Arc (fresh-frozen brains) or the entire forebrain (perfused brains) on a CM3050 S cryostat (Leica Microsystems, Nussloch GmbH, Germany). Sections from fresh-frozen brains were thaw-mounted on Superfrost Plus glass slides (Fisher Scientific Co., Pittsburgh, PA) and stored at −80 °C. Sections from perfused brains were collected free-floating in cryoprotectant (30% ethylene-glycol; 25% glycerol; 0.05 M PB), and stored at −20 °C. One-in-seven series of 16-μm thick sections were collected from the brains in Experiment 1 and one-in-five series of 20-μm thick sections were collected in Experiments 2—4.

2.9. Fluorescence *in situ* hybridization (FISH)

Pomc FISH. Free-floating sections containing the Arc (15—16 sections per brain) were transferred from cryoprotectant to PBS, mounted on Superfrost Plus slides, and desiccated overnight at 42 °C. The sections were hybridized with a digoxigenin-labeled antisense riboprobe corresponding to the full-length mouse *Pomc* mRNA (NCBI GenBank accession numbers NM_001278584.1), as described previously for PFA-perfused brains [28]. After stringent washes, 0.5% Triton X-100/0.5% H_2O_2 treatment and a 10 min incubation in 1% blocking reagent for nucleic acid hybridization (Roche Applied Sciences), the sections were incubated overnight in peroxidase-conjugated antidigoxigenin Fab fragments (Millipore Sigma, Burlington, MA; diluted 1:100 in 1% blocking reagent). Signal amplification was performed for 30 min using the TSA Biotin Tyramide system (PerkinElmer, Waltham, MA), and detected with Alexa Fluor 488-conjugated streptavidin (diluted 1:500 in 1% blocking reagent, Thermo Fisher). Fresh-frozen sections from the 16-day group in Experiment 4 were hybridized as already described for fresh-frozen brains [28], using reduced (15 min) tyramide amplification time.

Rax FISH. Sections were hybridized as per protocol for fresh-frozen brains [28], using a digoxigenin-labeled 1030 base long antisense probe corresponding to the entire coding region of mouse *Rax* mRNA (276—1304 bases of NM_013833.2). The template DNA was synthesized and cloned into pBluescript KS(−) plasmid by GenScript (Piscataway, NJ). Signal amplification was applied for 30 min, using the TSA Plus Biotin kit (PerkinElmer) with the TSA Plus biotin reagent diluted 1:400 in 0.05 M Tris and 0.01% H_2O_2. The biotin deposits were detected with Alexa Fluor 488-conjugated streptavidin.

2.10. Post-FISH immunofluorescence

Following *Pomc* FISH, brains with the *Synaptophysin-tdTomato* (*Ai34D*) allele were processed for immunofluorescence, with overnight incubation in the cocktail of a rabbit red fluorescent protein (RFP) antibody (1:400 dilution; Rockland Cat# 600-401-379, RRID:AB_2209751) that recognizes the tdTomato protein, and either a mouse monoclonal HuC/D antibody (2 μg/ml concentration; ThermoFisher Cat# A21271, RRID:AB_221448) or a Guinea pig NeuN antibody (1:2K dilution; Millipore Cat# ABN90, RRID:AB_11205592), to confirm neuronal identity. The primary antibodies were detected with Cy3-conjugated anti-rabbit and Alexa Fluor 647-conjugated anti-mouse or anti-Guinea pig IgGs (1:200 dilution each; Jackson Immunoresearch, West Grove, PA). Sections were coverslipped with SlowFade™ Diamond Antifade Mountant with DAPI (Thermo Fisher).

2.11. Immunofluorescence (IF)

Single IF for RAX. Fresh-frozen sections on slides (Experiment 1) were fixed with 4% PFA in 0.1 M PB (pH 7.4) for 15 min, then permeabilized with 0.5% Triton-X-100 for 20 min, and blocked with antibody diluent (2% normal horse serum, 0.2% Kodak Photo-Flo, 0.2% sodium-azide in PBS) for 20 min. Sections were incubated overnight in Guinea pig anti-RAX antibody (1:5 K dilution; RIKEN Institute for Developmental Biology Cat# MS8407-3, RRID:AB_2783560; gift from Dr. Hidetaka Suga, Nagoya University Graduate School of Medicine, Japan), followed by incubation in Cy3-conjugated anti-Guinea pig IgG (1:200) for 2 h. In preliminary experiments, this antibody yielded the same immunostaining pattern as a commercial Guinea pig RAX antibody (Cat# M229, Takara Bio Inc., Shiga, Japan; RRID: AB_2783559), but with slightly higher sensitivity.

Dual IF for RAX/MCT8 and RAX/HuC. Free-floating sections of *Rax-CreERT2/+:Ai34D* mice from Experiment 4 (7-day group; 1 male, 2 female) were treated with 0.5% Triton-X-100 for 30 min, rinsed in PBS (3 × 10 min), and blocked with antibody diluent for 20 min. The sections were incubated for 2 days in a cocktail of the Guinea pig RAX antibody (1:1K) and either a rabbit monocarboxylate transporter 8 (MCT8) antiserum (1:2K dilution; Visser TJ lab Erasmus University Medical Center, The Netherlands, Cat# 1306; RRID:AB_2661880; a gift from Dr. Theo J. Visser) or a biotinylated anti-HuC/D antibody (5 μg/ml concentration; Thermo Fisher Scientific, Cat# A-21272, RRID:AB_2535822). The unconjugated primary antibodies were detected with Alexa Fluor 647 anti-Guinea pig and Alexa Fluor 488 anti-rabbit (1:200 each) for 2 h. The biotinylated HuC/D antibody was detected with avidin-biotin-peroxidase complex (1:500 dilution for 2 h; Elite ABC-HRP Kit, Vector, Burlingame, CA), followed by 15 min biotin-tyramide amplification and fluorescein (DTAF) streptavidin (1:300 dilution, Jackson Immunoresearch).

Dual IF for POMC/α-MSH. Sections from Experiments 2 and 4 were treated with 0.5% Triton X-100 and 0.5% H_2O_2 for 15 min, blocked with antibody diluent for 20 min, and incubated in the cocktail of rabbit anti-POMC (1:15K dilution; Phoenix Pharmaceuticals, Cat# H-029-30, RRID:AB_2307442) and sheep anti-α-MSH (1:20K dilution; Millipore, Cat# AB5087, RRID:AB_91683; gift of Jeffrey B. Tatro, Tufts Medical Center, Boston MA) antisera for 22 h at room temperature. The primary antibodies were detected with Alexa Fluor 647 anti-rabbit and Alexa 488 anti-sheep IgGs (1:200 each) for 2 h. In Experiment 3, to eliminate high lipofuscin autofluorescence, sections were incubated in 0.3% Sudan Black B (Sigma—Aldrich) in 70% ethanol for 10 min, followed by a vigorous wash in 70% ethanol for 5 min, before the antibody diluent step. Sections from Experiment 3 were incubated for 24 h in the cocktail of 1:10K POMC and 1:20K anti-α-MSH antisera, and subsequently, in Cy3-conjugated anti-rabbit and Alexa 488 anti-sheep IgGs (1:200 each) for 2 h. Sections were mounted and coverslipped with SlowFade™ Diamond Mountant with DAPI.

2.12. Image acquisition and analysis

All images were captured with a Zeiss Axioplan 2 epifluorescent microscope (Carl Zeiss, Göttingen, Germany) equipped with an RT SPOT digital camera (Diagnostic Instruments, Sterling Heights, MI). Cell counts (RAX IF, *Pomc* FISH, POMC IF, including dual-labeling with tdTomato), were carried out manually on every 5th coronal 20 μm thick section covering the entire rostrocaudal length of tanycyte and POMC neuron distribution (retrochiasmatic area and Arc, 15—16 sections per brain; the same number also for fresh-frozen collected sections in the 16-day group in Experiment 4). Because of partial tissue loss of the Arc, one male *Rax-CreERT2/*+:Arc*Pomc^{loxTB/loxTB}* brain in Experiment 3 was excluded from the *Pomc* cell count, but was included in the POMC IF fiber analysis. Semiquantitative analysis of POMC fibers was performed using ImageJ software (public domain at http://rsb.info.nih.gov/ij). Images were acquired from each region bilaterally in two consecutive sections (in a one-in-five section series) using a $10\times$ objective. POMC-labeled fibers were separated from the background using the same threshold value for all images and the %Area covered by POMC fibers was measured. Nonspecific signals such as artifacts or labeling of blood vessels in some brains were removed manually. % Area values were expressed as a percentage of the %Area measured in WT and *Rax-CreERT2/*+brains in Experiments 2 (n = 2 males, 2 females) and 3 (n = 2 males, 3 females).

2.13. Statistics

GraphPad Prism 8 software was used to calculate statistics and plot graphs. All data are presented as mean ± SEM. Datasets were tested for normality by using the Shapiro—Wilk (when n < 8) or D'Agostino—Pearson normality tests. Comparisons between *Pomc* cell counts or POMC fiber densities were made using a two-tailed unpaired t-test or one-way analysis of variance (ANOVA) followed by Tukey's multiple comparisons test, or Mann—Whitney test for non-Gaussian data distributions. In the metabolic study, the differences in bodyweights and other parameters were tested for significance using one-way ANOVA followed by Tukey's multiple comparisons test. In the age cohort experiment, bodyweight gains were compared using Welch's ANOVA followed by Dunnett's T3 multiple comparisons test. To correlate bodyweight gains with *Pomc* cell counts, the Pearson correlation (*r*) was calculated with a two-tailed *p*-value. Differences were considered significant for *p* < 0.05. The number of mice (n) per group, statistical tests used, and *p* values are described in the Results or figure legends.

3. RESULTS

3.1. Distribution of Rax/RAX+ cells in the mediobasal hypothalamus

Rax has been regarded as a tanycyte-specific marker in the postnatal and adult hypothalamus [17—20]. To identify all potential *Rax*+ progenitors in the hypothalamus, we examined the distribution of *Rax*+ cells using FISH for *Rax* mRNA, and IF for the transcription factor it encodes, retinal homeobox protein Rx (RAX) that is localized in cell nuclei. In agreement with previous studies [18,29], the vast majority of *Rax*-expressing cells corresponded to the distribution of tanycytes in the third ventricular wall and the median eminence (Figure 1C—E). A minor but conspicuous population of *Rax*+ cells was also observed in the parenchyma of the caudal Arc (caudal of Bregma −2.30 mm; Figure 1E), but only a few scattered *Rax*+ cells were found in the parenchyma alongside the rostral and mid portions of the tanycyte region (Figure 1C,D). RAX immunostaining labeled cell nuclei in the same distribution pattern as *Rax* mRNA, including parenchymal cells (Figure 1F—H).

3.2. RAX is expressed in tanycytes, tanycyte-like cells, and a distinct glial cell type in the hypothalamic parenchyma

To examine the morphology of parenchymal RAX+ cells, we performed RAX immunolabeling in hypothalamic sections from TAM-treated *Rax-CreERT2/*+:Ai34D mice. In these mice, TAM-induced CreERT2 activates the floxed *Synaptophysin-tdTomato* fusion protein reporter allele under transcriptional control of the constitutively active CAG promoter, resulting in synaptophysin-tdTom expression in the entire cytoplasm of RAX+ cells and their progeny. Seven days after the first TAM injection, synaptophysin-tdTom labeled cell bodies and processes of tanycytes, corresponding to the distribution of RAX, were observed (Figure 2). Of the RAX+ cells counted in the parenchyma (122 ± 21 cells total, n = 3 mice; 4.2 ± 0.6 and 18.1 ± 2.6 cells per section rostral and caudal from Bregma −2.30 mm, respectively), about half (49.2 ± 2.8%) did not express any detectable synaptophysin-tdTom. The other half that expressed synaptophysin-tdTom in their cytoplasm could be roughly classified into two morphological types: one with size and shape similar or virtually identical to tanycytes (16.4 ± 6.0% of all parenchymal RAX+ cells) (Figure 2B1-2, C1-3); and another with a different, nonelongated shape characterized by the extension of fine processes, often making the cells appear as large patches (34.4% ± 3.4%) (Figure 2B1-2, D-F). The processes of these cells, which will be referred to as "frizzy cells", often encircled the cell bodies of adjacent neurons (Supplementary Fig 1B1-4 and Figure 2E1-E3). Morphologically, frizzy cells were most reminiscent of protoplasmic astrocytes observed in the brainstem [30]; however, they were negative for GFAP immunostaining and the tanycyte markers, vimentin and MCT8 (Supplementary Fig. 2). The vast majority of frizzy RAX+ cells were found in the caudal Arc (Figure 2D), while few were observed rostral to Bregma −2.30 mm, in the dorsomedial (DMH) and ventromedial nuclei (VMH) of the hypothalamus, and the lateral Arc. We often observed doublets of RAX-positive nuclei that belonged to frizzy cells (Figure 2F2, Supplementary Fig 1B2), suggesting recent cell divisions. We also observed numerous frizzy synaptophysin-tdTom+ cells of the same or very similar morphology that lacked RAX staining, indicating the downregulation of *Rax* expression after the induction of synaptophysin-tdTomato reporter expression. These cells were more broadly distributed—not only in the caudal Arc (Figure 2D1), but also more rostrally in the DMH, VMH, and lateral Arc (Figure 2B1) and spreading out laterally as far as the lateral hypothalamus, often adjacent to the meninges (Supplementary Fig. 1A). While the mean lateral distance of RAX+ frizzy cells from the third ventricle was 209 ± 9 μm (n = 109 cells, from 3 mice) and the maximum was 433 μm, RAX-negative frizzy cells had a mean distance of 407 ± 14 μm (n = 298 cells, from 3 mice) with 1120 μm as maximum distance, and 31% were farther than 500 μm from the third ventricle. Altogether, RAX-negative, frizzy tdTom+ cells were approximately three times more numerous than RAX-positive frizzy tdTom+ cells. Several RAX-negative frizzy tdTom+ cells were conspicuous in the hypothalamic paraventricular nucleus (PVH); they were occasionally observed as far rostral as the preoptic area (POA) and the bed nucleus of the stria terminalis (BNST). Importantly, RAX immunostaining was never observed in neurons identified by HuC immunofluorescence (Supplementary Fig 1B1-4).

It is important to note the different distribution of tdTomato+ tanycyte-like cells and frizzy cells, particularly at rostral and mid-levels of the Arc. Tanycyte-like cells were observed only in the medial portion of the Arc or VMH, a maximum of 200 μm away from the ventricle wall, in agreement with previous studies [31,32]. Frizzy cells were distributed more laterally, as they appeared to be largely excluded from the area dominated by the ventrolaterally arching tanycyte processes
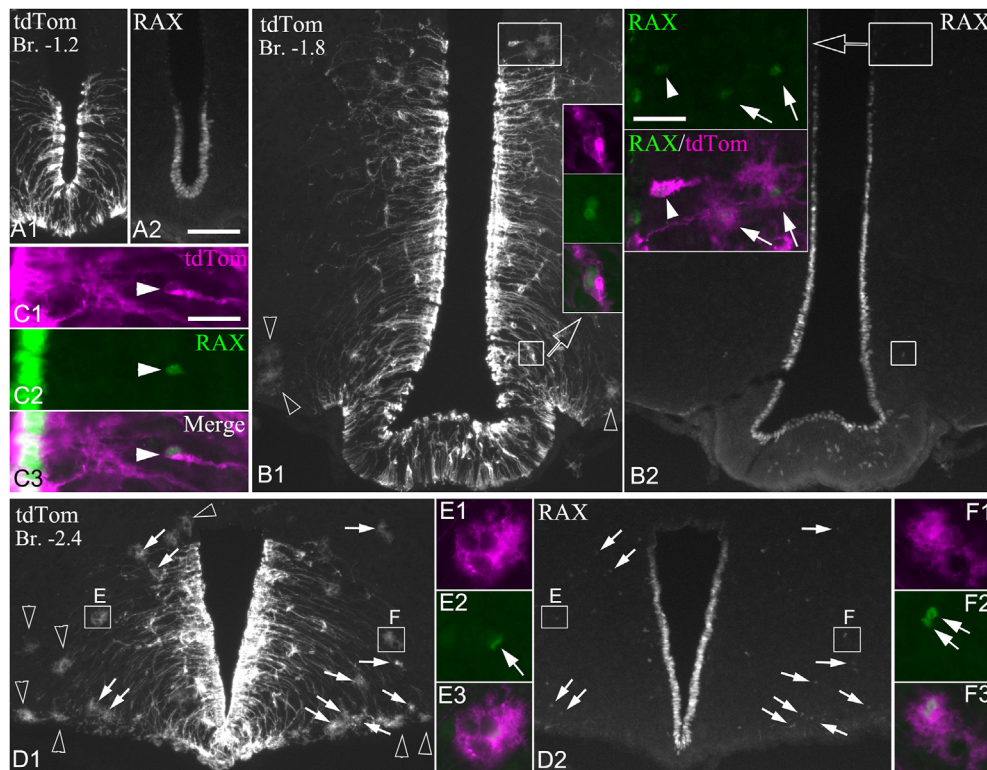
Figure 2: Morphology of parenchymal RAX cells as revealed by the synaptophysin-tdTomato reporter in *Rax-CreERT2/+:Ai34D* mice. (A1-2, **B1-2**, **D1-2)** Low magnification grayscale images show native tdTomato fluorescence (A1, B1, and D1) and RAX IF (A2, B2, and D2) of the same fields from rostral, mid, and caudal levels of the tanycyte region. In the wall of the 3rd ventricle, tdTomato-labeled tanycytes are distributed in the same pattern as RAX. In the parenchyma, arrows indicate tdTomato-labeled frizzy cells that are RAX positive, open arrowheads that are RAX negative. **(Insets, C1-3, E1-3, F1-3)** Higher magnification images show dual-labeled, tdTomato (magenta) and RAX (green) positive parenchymal cells. **B1 inset** shows two closely adjacent RAX cells in the Arc parenchyma with morphology similar to tanycytes. **B2 inset** shows a tanycyte translocated into the parenchyma (white arrowhead) and two frizzy cells (arrows) in the dorsomedial nucleus. **C1-3** shows a RAX positive cell well inside the Arc parenchyma (~Bregma −2.40 mm) with morphology identical to tanycytes. **E1-3** and **F1-3** show frizzy cells inside the boxed areas from **D1-2**. The double arrows in **F2** point to two adjacent RAX nuclei. Scale bars: 100 μm (**A2**, for all low magnification images); 25 μm (**B2 inset**); 25 μm (**C1-3**, for **B1 inset, E1-3, F1-3**). (For interpretation of the references to color in this figure legend, the reader is referred to the Web version of this article.)

(Supplementary Fig. 1A and E), except in the caudal Arc (caudal of Bregma −2.30 mm). Frizzy cells could be adjacent to the ventricle in the VMH (Supplementary Fig. 1C), but their distance from the ventricle increased to a minimum of ~120 μm at the dorsal border of the Arc (Supplementary Fig. 1D) and a minimum of ~170−180 μm in the Arc (Supplementary Fig. 1D and E). Frizzy cells were frequent in the lateral portion of the Arc, >200 μm from the ventricle wall (Supplementary Fig. 1E).

3.3. *Rax*⁺ progenitors give rise to *Pomc* neurons that develop normal efferent projections in young adult mice

The generation of new Arc *Pomc* neurons by *Rax*⁺ progenitors during early adulthood was assessed by *Pomc* FISH in *Rax-CreERT2/+:ArcPomc^loxTB/loxTB* mice that were injected with TAM at 4−5 weeks of age and euthanized 16 weeks later (Figure 1A,B). TAM-treated Arc*Pomc^loxTB/loxTB* littermates were used as negative controls, while WT and *Rax-CreERT2/+* littermates were used as positive controls. In Arc*Pomc^loxTB/loxTB* mice, very few Arc neurons had sufficient FISH signal to be counted as *Pomc* positive (Figure 3B1-5, E). The same was observed in the *Rax-CreERT2/+:ArcPomc^loxTB/loxTB* genotype without TAM treatment (data not shown). In all TAM-treated *Rax-CreERT2/+:ArcPomc^loxTB/loxTB* mice, a prominent population of *Pomc* neurons was observed in the Arc. The distribution of *Pomc* neurons in two *Rax-CreERT2/+:ArcPomc^loxTB/loxTB* brains that had the maximum and

minimum *Pomc* cell counts (186 and 72, respectively; counted on every 5th 20 μm thick Arc section) is illustrated in Figure 3C1-D5. Mean *Pomc* neuron counts were 125 ± 10 for males and 148 ± 12 for females (not significantly different, $t_{(12)} = 1.49$, $p = 0.161$, unpaired *t*-test), which amounted to approximately 10−12% of the normal *Pomc* neuron population observed in WT or *Rax-CreERT2/+* mice (Figure 3A1-5, F). The distribution of *Pomc* neurons was very similar in all *Rax-CreERT2/+:ArcPomc^loxTB/loxTB* mice: the majority were located in the medial Arc, <200 μm from the ventricle, and a smaller subset was located more laterally (Figure 3C1-D5). Few *Pomc* neurons were caudal of Bregma level −2.30 mm (Figure 3C5, D5).

The number of POMC neurons detected by IF in *Rax-CreERT2/+:ArcPomc^loxTB/loxTB* mice was ~70−75% of the numbers detected by FISH, but in the same distribution patterns (Figure 4A,B). POMC fibers in *Rax-CreERT2/+:ArcPomc^loxTB/loxTB* mice were observed in all major target regions of Arc POMC neurons, including the BNST, POA, PVH, DMH (Figure 4L−S, compared to normal fiber density in Figure 4D−G), lateral hypothalamus, medial amygdaloid nucleus, and thalamic paraventricular nucleus. POMC fiber densities in these regions varied greatly among *Rax-CreERT2/+:ArcPomc^loxTB/loxTB* brains, ranging from a moderate fiber density expected to arise from ~10% of the POMC neuron population to much lower densities or only sparse fibers. Brains with more *Pomc* neurons tended to have higher POMC fiber densities, but exceptions to this tendency were also observed. In general,
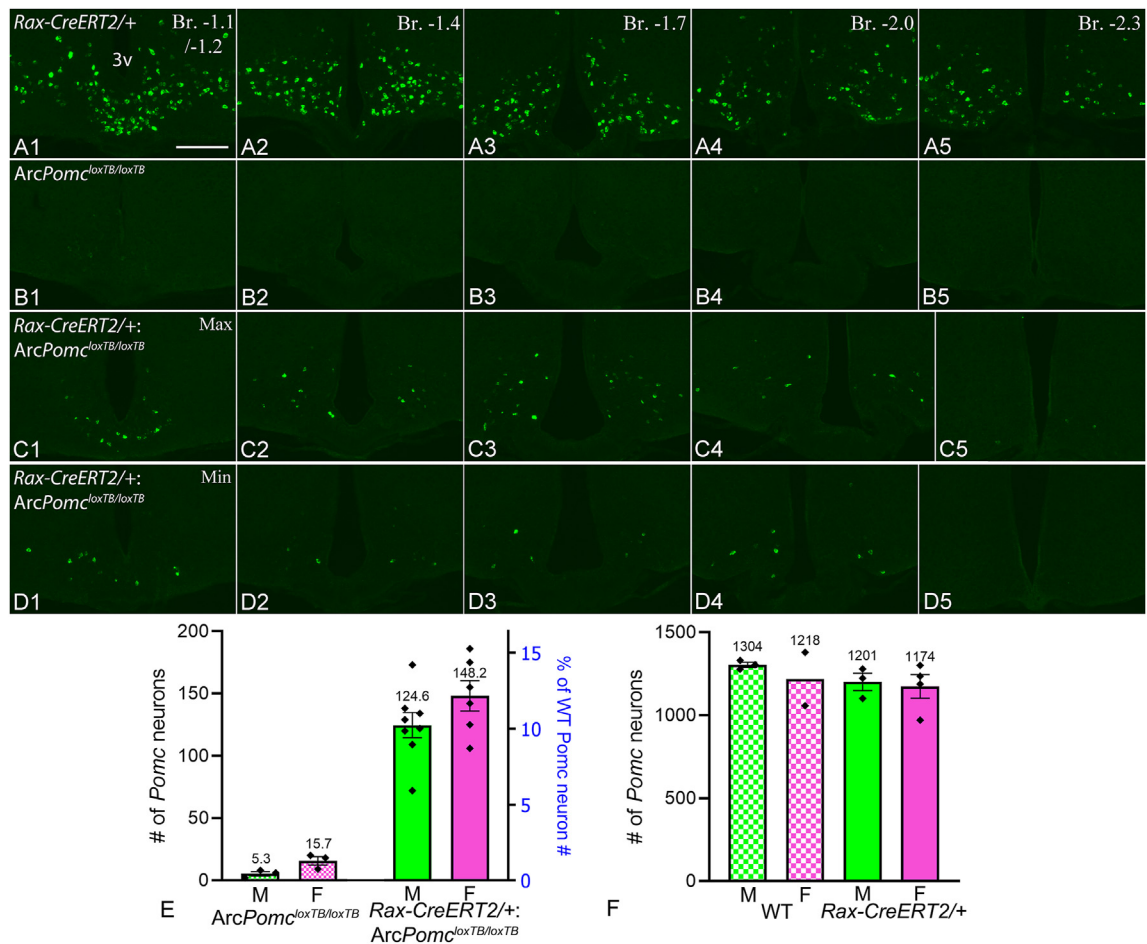
Figure 3: Distribution and quantification of hypothalamic *Pomc* neurons generated by *Rax*+ progenitors in early adult mice. (A1-5) FISH shows normal *Pomc* expression at 5 rostrocaudal levels of the Arc in a *Rax-CreERT2/+* mouse (positive control). **(B1-5)** *Pomc* neurons were barely detected by FISH in TAM-treated Arc*Pomc*$^{loxTB/loxTB}$ mice (negative control). **(C1-5, D1-5)** Distribution of *Pomc* neurons in two *Rax-CreERT2/+*:Arc*Pomc*$^{loxTB/loxTB}$ mice that were TAM-treated at 4−5 weeks of age and sacrificed 16 weeks later; C1-5 had the highest, D1-5 the lowest *Pomc* neuron count. *Rax-CreERT2/+*:Arc*Pomc*$^{loxTB/loxTB}$ images show all *Pomc* neurons in the sections; *Rax-CreERT2/+* images were cropped and do not show *Pomc* neurons in more lateral positions. **(E)** *Pomc* neuron counts in Arc*Pomc*$^{loxTB/loxTB}$ (n = 3 per sex) and *Rax-CreERT2/+*:Arc*Pomc*$^{loxTB/loxTB}$ mice (n = 8 males, n = 6 females). **(F)** *Pomc* neuron counts in male and female WT and *Rax-CreERT2/+* mice (n = 2−4); their combined average was used as 100% for scaling the right Y axis in **E**. Cell counts were made on every 5th, 20 μm thick coronal Arc section. 3v, third ventricle. Scale bar: 200 μm **(A1, for A1-D5)**.

females had more POMC fibers, and semiquantitative analysis revealed significantly higher POMC fiber density in females than males in the POA, PVH, and DMH (Figure 4C; BNST: $p = 0.0872$, POA: $p = 0.0080$, PVH: $p = 0.0080$, Mann−Whitney tests; DMH: $t_{(12)} = 2.749$, $p = 0.0176$ unpaired *t*-test). Similar to WT mice, practically all POMC fibers in *Rax-CreERT2/+*:Arc*Pomc*$^{loxTB/loxTB}$ mice were also immuno-positive for α-MSH (data not shown), which indicate normal proteolytic processing of POMC in these neurons. POMC fibers were virtually absent from the forebrain in Arc*Pomc*$^{loxTB/loxTB}$ mice (Figure 4H−K), as described previously [33].

3.4. *Rax-CreERT2/+*:Arc*Pomc*$^{loxTB/loxTB}$ mice have reduced fat mass, improved glucose tolerance, and insulin sensitivity than Arc*Pomc*$^{loxTB/loxTB}$ mice

In an attempt to understand the capacity of these newly generated POMC+ neurons in rescuing the obesity phenotype caused by the loss of Arc *Pomc* expression in Arc*Pomc*$^{loxTB/loxTB}$ mice, we performed the functional metabolic study outlined in Figure 1B. There was no significant difference in bodyweight for either sex between Arc*Pomc*$^{loxTB/loxTB}$ and *Rax-CreERT2/+*:Arc*Pomc*$^{loxTB/loxTB}$ mice over 16 weeks

(Figure 5A,H). However, there were significant differences in body composition (Figure 5); both male and female *Rax-CreERT2/+*:Arc*Pomc*$^{loxTB/loxTB}$ mice showed significantly reduced fat mass compared to Arc*Pomc*$^{loxTB/loxTB}$ mice (Figure 5B,E, I; male fat mass: $F_{(3, 25)} = 97.93$, $p < 0.0001$, one-way ANOVA; $p = 0.05$, Tukey's multiple comparisons; male fat mass%: $F_{(3, 25)} = 240.8$, $p < 0.0001$, one-way ANOVA; $p = 0.0009$, Tukey's multiple comparisons; female fat mass: $F_{(3, 18)} = 94.73$, $p < 0.0001$, one-way ANOVA; $p = 0.007$, Tukey's multiple comparisons). There were no significant differences in lean mass and fluid mass for either sex between Arc*Pomc*$^{loxTB/loxTB}$ and *Rax-CreERT2/+*:Arc*Pomc*$^{loxTB/loxTB}$ mice (Figure 5C,D, F, G, J, K, M, N). To examine glucose tolerance and insulin sensitivity, mice were subjected to oral glucose challenge after 5 h fasting. Before fasting, the blood glucose and plasma insulin levels were measured. *Rax-CreERT2/+*:Arc*Pomc*$^{loxTB/loxTB}$ male mice had significantly lower nonfasting plasma insulin levels compared with Arc*Pomc*$^{loxTB/loxTB}$ mice (Figure 6B; $F_{(3, 25)} = 13.17$, $p < 0.0001$, one-way ANOVA; $p = 0.024$, Tukey's multiple comparisons); with no differences in male and female nonfasting blood glucose (Figure 6A,I) and female non-fasting plasma insulin levels (Figure 6J). Following oral glucose
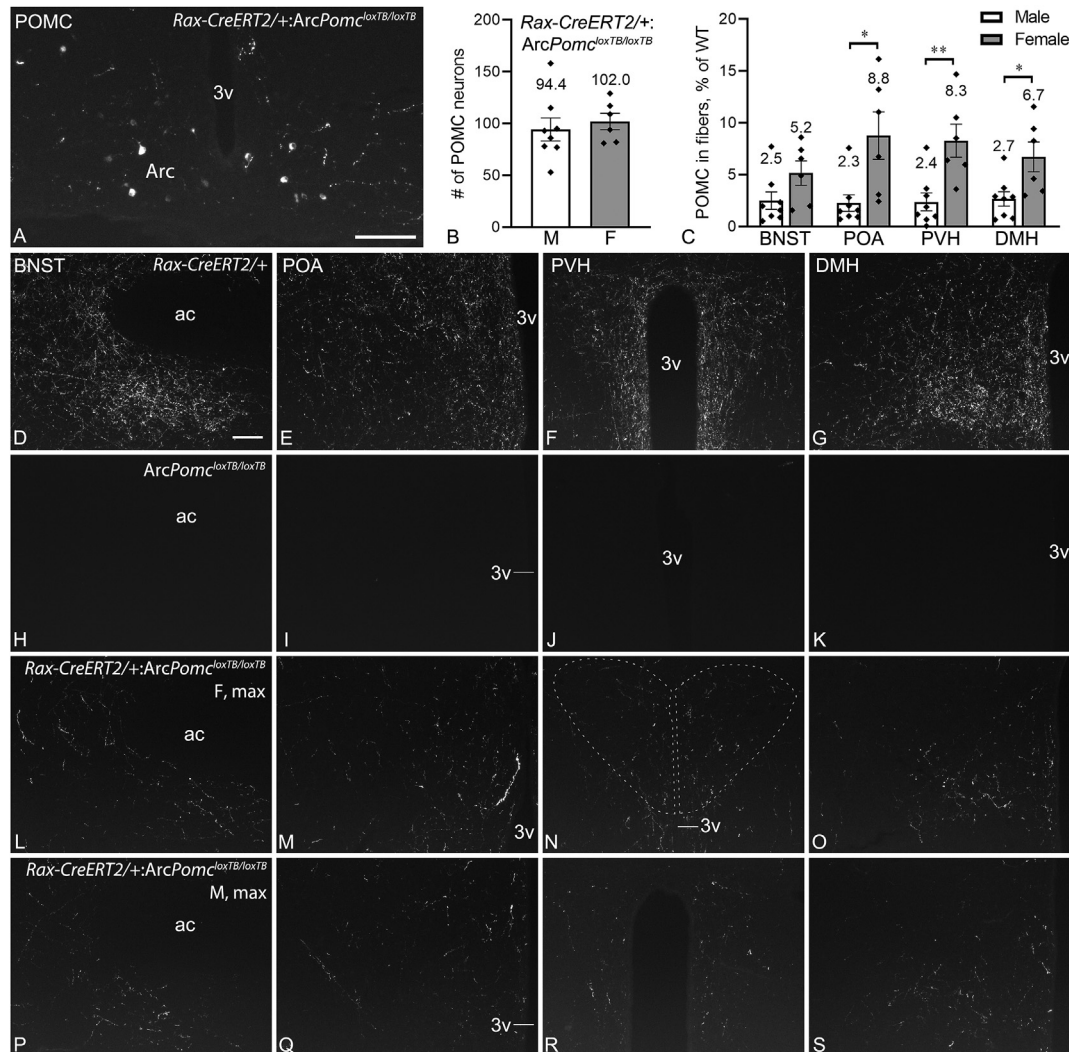
Figure 4: Immunofluorescent detection of *Rax*+ progenitor-derived POMC neurons and their efferents in young adult mice. (A) Cell bodies of POMC neurons in the rostral Arc of a *Rax-CreERT2/+*:Arc*Pomc*^loxTB/loxTB^ mouse. **(B)** POMC neuron counts in male (n = 8) and female (n = 6) *Rax-CreERT2/+*:Arc*Pomc*^loxTB/loxTB^ mice. **(C)** Quantification of POMC-immunoreactive fibers in the bed nucleus of the stria terminalis (BNST), preoptic area (POA), hypothalamic paraventricular nucleus (PVH), and dorsomedial nucleus (DMH) in *Rax-CreERT2/+*:Arc*Pomc*^loxTB/loxTB^ mice. Values (area% covered by POMC fibers) are expressed as % of WT; n = 8 males, n = 6 females; *$p < 0.05$, **$p < 0.01$; BNST: $p = 0.0872$, POA: $p = 0.0080$, PVH: $p = 0.0080$, Mann−Whitney tests; DMH: $p = 0.0176$, unpaired t-test. **(D−S)** POMC fibers shown in *Rax-CreERT2/+*(positive control; **D-G**), Arc*Pomc*^loxTB/loxTB^ (negative control; **H−K**), and female **(L−O)** and male **(P−S)** *Rax-CreERT2/+*:Arc*Pomc*^loxTB/loxTB^ mice with the highest POMC fiber densities in the quantified regions; BNST: **(D, H, L, P)**, POA: **(E, I, M, Q)**, PVH: **(F, J, N, R)**, DMH: **(G, K, O, S)**. 3v, third ventricle; ac, anterior commissure. Scale bars: 100 μm **(A)** and 100 μm **D**, for **D-S**).

challenge, male *Rax-CreERT2/+*:Arc*Pomc*^loxTB/loxTB^ mice showed significantly reduced blood glucose levels at 15 ($F_{(3, 25)} = 9.89$, $p = 0.0002$, one-way ANOVA; $p = 0.001$, Tukey's multiple comparisons) and 30 min ($F_{(3, 25)} = 6.03$, $p = 0.003$, one-way ANOVA; $p = 0.023$, Tukey's multiple comparisons), and significantly reduced plasma insulin levels at 0 ($F_{(3, 25)} = 13.16$, $p < 0.0001$, one-way ANOVA; $p = 0.024$, Tukey's multiple comparisons), 60 ($F_{(3, 25)} = 18.65$, $p < 0.0001$, one-way ANOVA; $p = 0.023$, Tukey's multiple comparisons), and 120 min ($F_{(3, 25)} = 13.98$, $p < 0.0001$, one-way ANOVA; $p = 0.006$, Tukey's multiple comparisons) compared with Arc*Pomc*^loxTB/loxTB^ mice (Figure 6C,D). In addition, male *Rax-CreERT2/+*:Arc*Pomc*^loxTB/loxTB^ mice showed significantly reduced calculated glucose AUC ($F_{(3, 25)} = 8.78$, $p = 0.0004$, one-way ANOVA; $p = 0.023$, Tukey's multiple comparisons), calculated insulin AUC ($F_{(3, 25)} = 22.28$, $p < 0.0001$, one-way ANOVA; $p = 0.012$, Tukey's multiple comparisons), glucose-insulin index ($F_{(3, 25)} = 13.69$,

$p < 0.0001$, one-way ANOVA; $p = 0.007$, Tukey's multiple comparisons), and HOMA-IR index (measure of insulin resistance; $F_{(3, 25)} = 10.01$, $p = 0.0002$, one-way ANOVA; $p = 0.047$, Tukey's multiple comparisons) compared with Arc*Pomc*^loxTB/loxTB^ mice (Figure 6E−H). Similarly, female *Rax-CreERT2/+*:Arc*Pomc*^loxTB/loxTB^ mice showed significantly reduced calculated insulin AUC ($F_{(3, 17)} = 38.53$, $p < 0.0001$, one-way ANOVA; $p = 0.006$, Tukey's multiple comparisons) and glucose-insulin index ($F_{(3, 17)} = 19.65$, $p < 0.0001$, one-way ANOVA; $p = 0.014$, Tukey's multiple comparisons) compared with Arc*Pomc*^loxTB/loxTB^ mice (Figure 6N, O). There were no differences in blood glucose and plasma insulin levels over time, calculated glucose AUC, and HOMA-IR index in females (Figure 6K-M, P).

The average daily food intake measured at age 14 and 15 weeks did not differ between genotypes (Supplementary Fig. 3A and C). Furthermore, a fasting-refeeding experiment performed at age 15
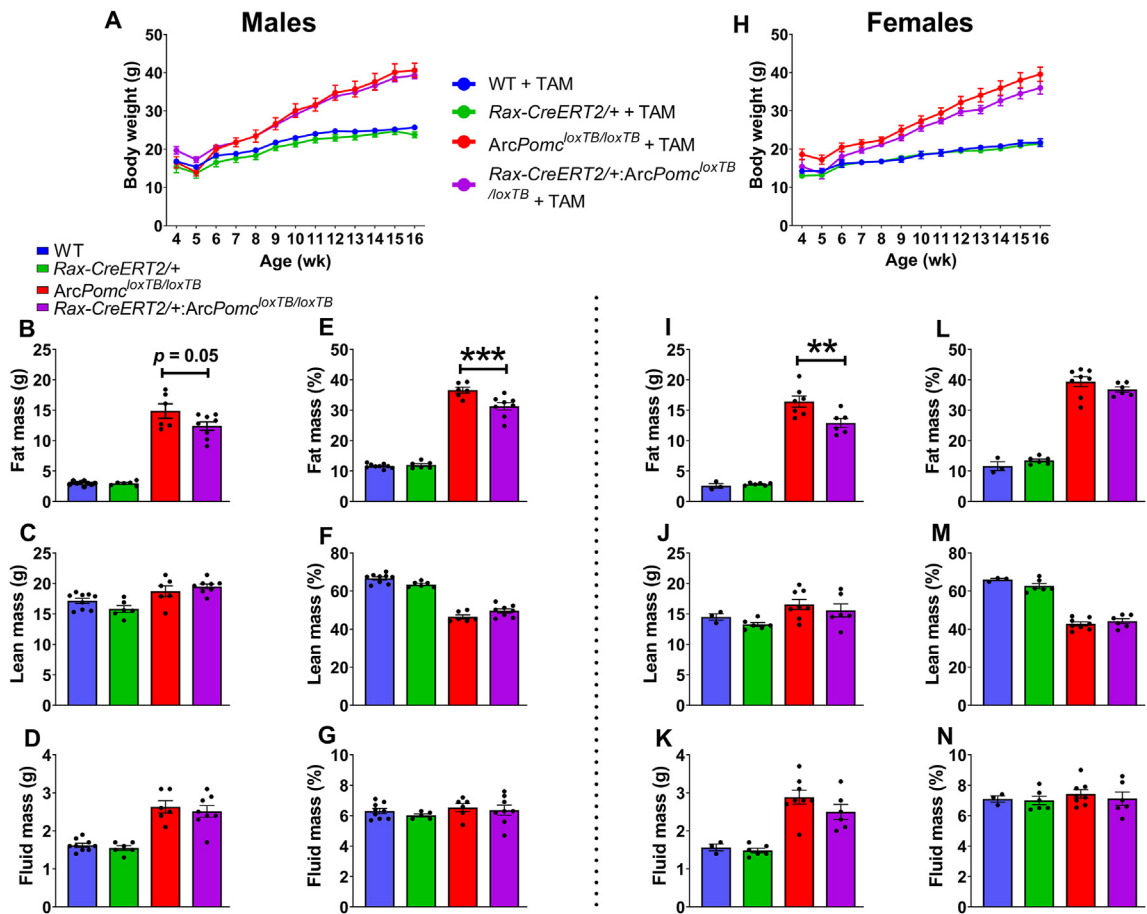
Figure 5: *Rax-CreERT2*:Arc*Pomc*^{loxTB/loxTB} mice show significantly reduced fat mass compared to Arc*Pomc*^{loxTB/loxTB} mice. **(A, H)** Bodyweight growth curves of males and females following TAM treatment. There was no significant change in bodyweight between Arc*Pomc*^{loxTB/loxTB} and *Rax-CreERT2*:Arc*Pomc*^{loxTB/loxTB} mice over 16 weeks ($p > 0.05$, one-way ANOVA; Tukey's multiple comparisons). Body composition - Fat mass **(B, I)**; lean mass **(C, J)**; and fluid mass **(D, K)** of male **(B–D)** and female **(I–K)** mice analyzed by NMR. **(E-G, L-N)** Body composition mass measurements are shown as a percentage of total body mass. *Rax-CreERT2/*+:Arc*Pomc*^{loxTB/loxTB} mice show reduced fat mass (males: $p = 0.05$, females: **$p = 0.007$; Tukey's multiple comparisons), and reduced fat mass% in males (***$p = 0.0009$; Tukey's multiple comparisons) compared to Arc*Pomc*^{loxTB/loxTB} mice. Data are shown as mean ± SEM (males, n = 6−9/group; females, n = 3−8/group). Individual mouse values are represented by filled circles. The data were analyzed using one-way ANOVA followed by Tukey's multiple comparisons test.

weeks showed the normal compensatory hyperphagic response to an 18-h fast and return of bodyweight to baseline without any genotype or sex differences (Supplementary Fig. 3).

3.5. *Pomc* neurons continuously arise from *Rax*⁺ progenitors at least until senescence

To determine whether *Rax*⁺ progenitors continue to generate new *Pomc* neurons after early adulthood, we performed *Pomc* FISH in different age groups (8 cohorts) of *Rax-CreERT2*:Arc*Pomc*^{loxTB/loxTB} mice that received TAM treatment between ages 15−50 weeks, and were euthanized either 12 weeks (cohort 3) or 14−16 weeks (all other cohorts) later (Figure 7A). The two oldest cohorts (cohorts 7 and 8) were euthanized at 14−15 months of age, which is considered the end of middle age in mice [34]. TAM-treated Arc*Pomc*^{loxTB/loxTB} littermates were used as negative controls and *Rax-CreERT2/*+littermates were used as positive controls. The number of *Pomc* neurons across these age groups was very similar to that observed in early adult *Rax-CreERT2/*⁺:Arc*Pomc*^{loxTB/loxTB} mice (males: 129 ± 9; females: 147 ± 9) (Figure 7A,B). This amounted to ~9−10% of the normal *Pomc* neuron number counted in *Rax-CreERT2/*+ littermates, which

was somewhat higher than in early adult *Rax-CreERT2/*+ or WT mice (Figure 7C; compare to Figure 3F). There was no difference in the number of *Pomc* neurons between the 12 and 16 weeks survival time after TAM treatment (Figure 7A). Brains with the highest *Pomc* neuron counts from cohorts 3, 5, and 8 are shown in Figure 7D1-F5.

POMC/α-MSH IF was performed in all *Rax-CreERT2/*+:Arc*Pomc*^{loxTB/loxTB} mice (except cohort 3) to study the distribution of POMC fibers. POMC fibers were observed in all major projection regions, including BNST, POA, PVH, and DMH (Supplementary Fig. 4E-L, compared to normal fiber density in A-D). POMC fiber densities in these regions were similar to that observed in early adult *Rax-CreERT2/*+:Arc*Pomc*^{loxTB/loxTB} mice, although the highest fiber densities remained lower compared with early adults. Female mice had significantly higher densities of POMC fibers than males in all measured regions (Figure 7G; BNST: $t_{(18)} = 2.84$, $p = 0.0108$, DMH: $t_{(18)} = 3.72$, $p = 0.0016$, POA: $t_{(18)} = 3.00$, $p = 0.0077$, unpaired *t*-tests; PVH: $p = 0.0077$, Mann−Whitney test).

Bodyweight gain at 12 weeks after TAM treatment, combined from cohorts 1−6, are shown in Figure 7H (cohorts 7 and 8 were excluded from this analysis due to higher likelihood of age-related bodyweight
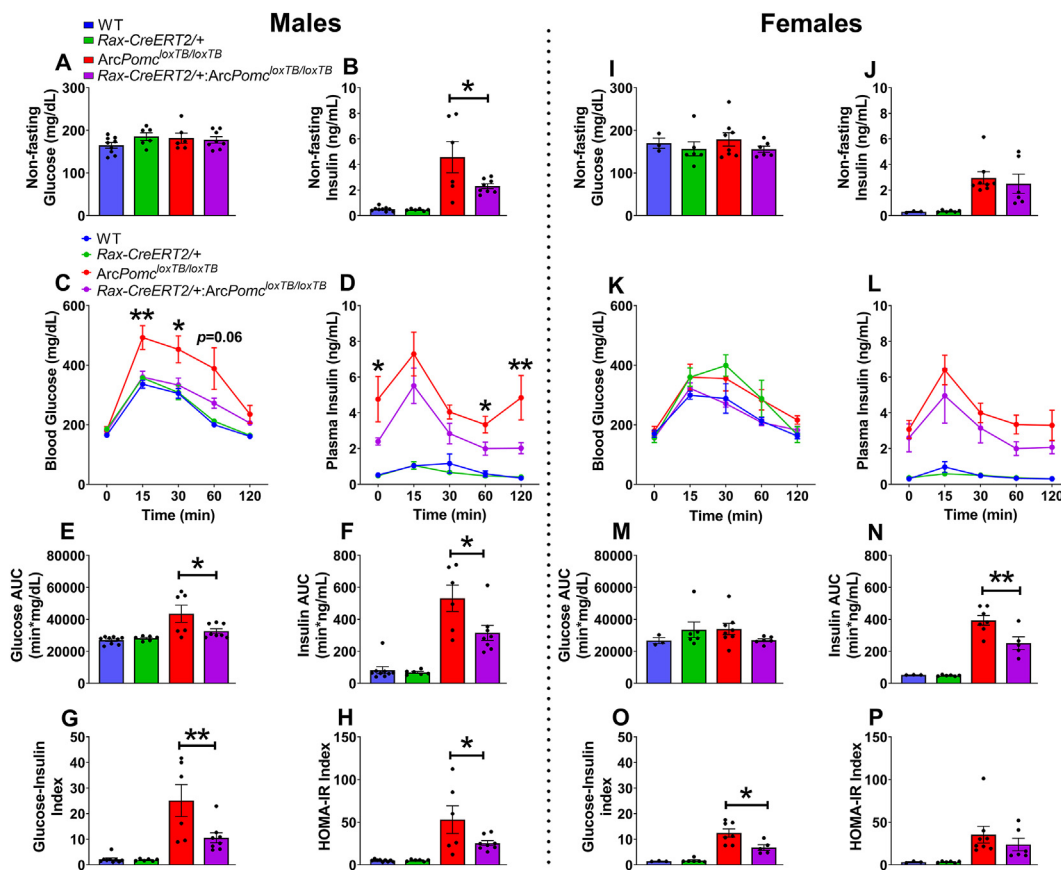
Figure 6: *Rax-CreERT2*:Arc*Pomc$^{loxTB/loxTB}$* **mice show significantly improved glucose tolerance and insulin sensitivity compared to Arc*Pomc$^{loxTB/loxTB}$* mice in response to an oral glucose tolerance test. (A, I)** Blood glucose levels before fasting in male and female mice, measured using a glucometer. There was no significant difference in nonfasting blood glucose levels between the groups for either sex. **(B, J)** Plasma insulin levels before fasting in male and female mice, measured by ELISA. *Rax-CreERT2/+*:Arc*Pomc$^{loxTB/loxTB}$* male mice show lower nonfasting plasma insulin levels (*$p = 0.024$; Tukey's multiple comparisons) compared to Arc*Pomc$^{loxTB/loxTB}$* mice. **(C, K)** *Rax-CreERT2*:Arc*Pomc$^{loxTB/loxTB}$* male, but not female, mice show significantly reduced blood glucose levels at 15 (**$p = 0.001$, Tukey's multiple comparisons) and 30 min (*$p = 0.023$, Tukey's multiple comparisons) after oral glucose challenge, compared to Arc*Pomc$^{loxTB/loxTB}$* mice. **(D, L)** *Rax-CreERT2*:Arc*Pomc$^{loxTB/loxTB}$* male, but not female, mice show significantly reduced plasma insulin levels at 0 (*$p = 0.024$, Tukey's multiple comparisons), 60 (*$p = 0.023$, Tukey's multiple comparisons), and 120 min (**$p = 0.006$, Tukey's multiple comparisons) after oral glucose challenge, compared to Arc*Pomc$^{loxTB/loxTB}$* mice. **(E, M)** *Rax-CreERT2*:Arc*Pomc$^{loxTB/loxTB}$* male, but not female mice, show significantly reduced glucose areas under the curve (AUC; *$p = 0.023$, Tukey's multiple comparisons) compared to Arc*Pomc$^{loxTB/loxTB}$* mice. **(F, N)** *Rax-CreERT2*:Arc*Pomc$^{loxTB/loxTB}$* male and female mice show significantly reduced insulin areas under the curve (AUC; male: *$p = 0.012$, female: **$p = 0.006$; Tukey's multiple comparisons) compared to Arc*Pomc$^{loxTB/loxTB}$* mice. **(G, O)** *Rax-CreERT2*:Arc*Pomc$^{loxTB/loxTB}$* male and female mice show significantly reduced glucose-insulin indexes (male: **$p = 0.007$, female: *$p = 0.014$; Tukey's multiple comparisons). **(H, P)** *Rax-CreERT2*:Arc*Pomc$^{loxTB/loxTB}$* male, but not female, mice show significantly reduced HOMA-IR indexes (*$p = 0.047$, Tukey's multiple comparisons) compared to Arc*Pomc$^{loxTB/loxTB}$* mice. Data are shown as mean ± SEM (males, n = 6−9/group; females, n = 3−8/group). Individual mouse values are represented by filled circles. The data were analyzed using one-way ANOVAs followed by Tukey's multiple comparisons test.

loss, independent of genotype). The initial pre-TAM bodyweights of *Rax-CreERT2/+*:Arc*Pomc$^{loxTB/loxTB}$* and Arc*Pomc$^{loxTB/loxTB}$* mice were characteristic of obesity in all age coorts (from 40.2 ± 1.6 g in the younger cohort 1 to 65.8 ± 2.5 g in the 27-week-old cohort 6). *Rax-CreERT2/+*:Arc*Pomc$^{loxTB/loxTB}$* mice gained significantly less weight than Arc*Pomc$^{loxTB/loxTB}$* mice (0.7 ± 1.8 g *vs* 9.3 ± 1.8 g; $W_{(2.00, 13.18)} = 8.885$, $p = 0.0036$, Welch's ANOVA; $p = 0.0114$, Dunnett's T3 multiple comparisons); several *Rax-CreERT2/+*:Arc*Pomc$^{loxTB/loxTB}$* mice lost weight up to 16 g (Figure 7H). Bodyweight gain in *Rax-CreERT2/+*:Arc*Pomc$^{loxTB/loxTB}$* mice negatively correlated with the number of *Pomc* neurons observed in these mice (Figure 7I; Pearson $r = -0.64$, $p = 0.0019$, n = 21). When analyzed separately by sex, the negative correlation was statistically significant in females ($r = -0.75$, $p = 0.0123$, n = 10), but not in males ($r = -0.48$, $p = 0.1352$, n = 11) (Figure 7I).

3.6. New *Pomc* neurons are generated rapidly from *Rax$^+$* progenitors

The previous results that showed no difference in *Pomc* neuron counts in mice sacrificed 12 or 16 weeks after TAM treatment suggested that *Pomc* neurons derived from *Rax$^+$* progenitors may not accumulate linearly with time. To study the dynamics of *Pomc* neuron generation by *Rax$^+$* progenitors during shorter intervals, we performed *Pomc* FISH on *Rax-CreERT2/+*:Arc*Pomc$^{loxTB/loxTB}$* mice sacrificed at 7 (7-day group) or 16 (16-day group) days following the first TAM injection (Figure 8A1-B5). At 7 days, we counted 56 ± 8 *Pomc* neurons (n = 8; 3 males, 5 females), which is equivalent to ~42% of the *Pomc* neurons observed in mice sacrificed 16 weeks after TAM induction in the early adult experiment (Figure 8C). At 16 days, 131 ± 30 *Pomc* neurons were counted (n = 4; 3 males, 1 female), which is identical to the number observed 16 weeks after TAM treatment (Figure 8C). These
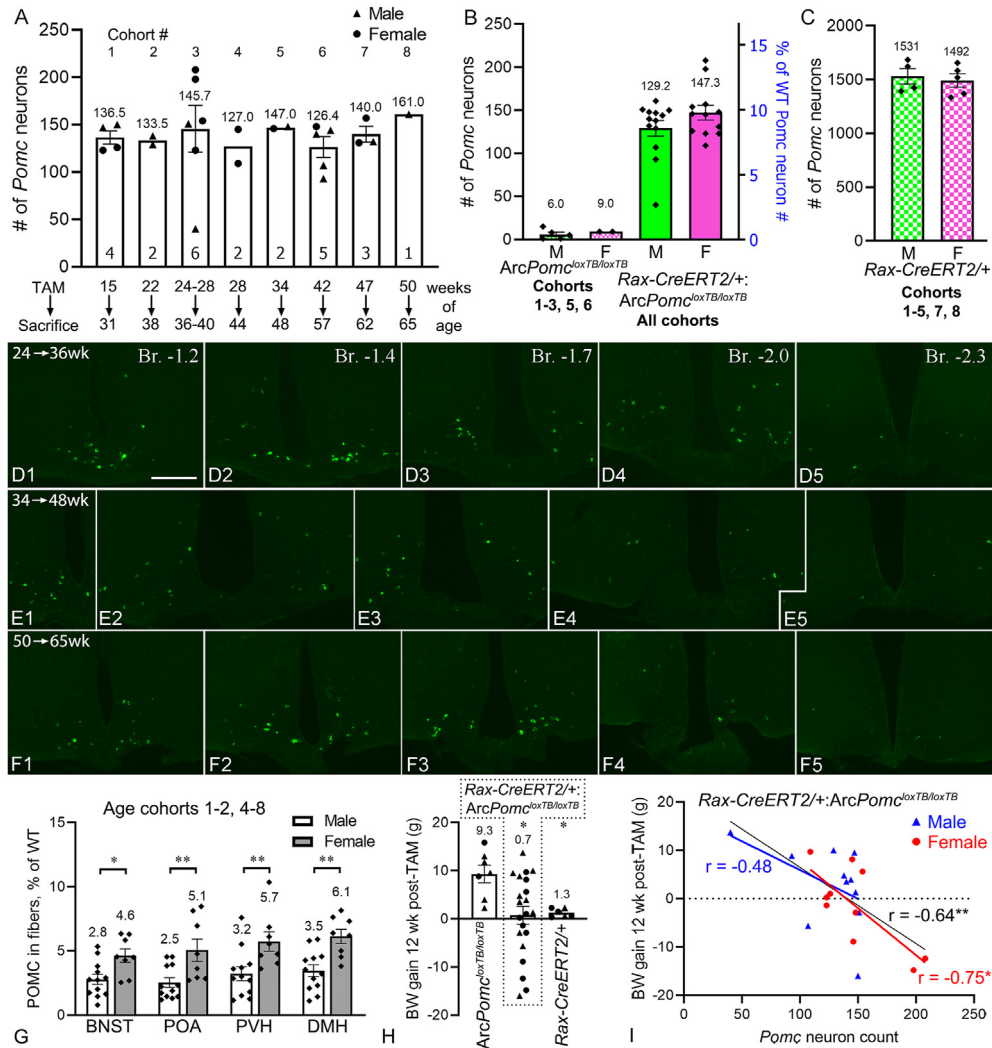
Figure 7: Generation of hypothalamic *Pomc* neurons by *Rax*⁺ progenitors in mature adult and middle aged mice. (A) *Pomc* neuron counts in 8 different age cohorts of *Rax-CreERT2/+:ArcPomc^loxTB/loxTB* mice that were perfused at either 12 week (cohort 3) or 14—16 weeks (all other cohorts) after TAM treatment. Sample sizes are shown inside the columns. **(B)** *Pomc* neuron counts in male (n = 13) and female (n = 12) *Rax-CreERT2/+:ArcPomc^loxTB/loxTB* mice from all cohorts combined (male *vs* female not significantly different, $p = 04777$, Mann—Whitney test); and male (n = 5) and female (n = 2) ArcPomc^loxTB/loxTB mice (negative controls) from 5 cohorts (n = 1—2 each). **(C)** *Pomc* neuron counts in male (n = 4) and female (n = 5) *Rax-CreERT2/+* mice (positive controls) from 7 cohorts (n = 1—2 each); their combined mean was used as 100% for scaling the right Y axis in **B**. **(D1-F5)** Distribution of *Pomc* neurons (FISH) in *Rax-CreERT2/+:ArcPomc^loxTB/loxTB* brains with the highest *Pomc* neuron counts from cohort 3 **(D1-5)**, cohort 5 **(E1-5),** and cohort 8 **(F1-5)**. Five rostrocaudal levels are shown for each cohort. Images show all *Pomc* neurons in the sections. Note that several *Pomc* neurons are in very lateral positions in **E1-5**; the most lateral is ~600 μm away from the ventricle in **E4**. **(G)** Semiquantitative analysis of POMC fiber staining in male (n = 12) and female (n = 8) *Rax-CreERT2/+:ArcPomc^loxTB/loxTB* mice from all age cohorts except cohort 3. Values (area% covered by POMC fibers) are expressed as % of WT. *$p < 0.05$, **$p < 0.01$; BNST: $p = 0.0108$, DMH: $p = 0.0016$, POA: $p = 0.0077$, unpaired *t*-test; PVH: $p = 0.0077$, Mann—Whitney test. **(H)** Bodyweight gains at 12 weeks after TAM injection in cohorts 1—6; *significantly different from ArcPomc^loxTB/loxTB. $W_{(2.00,13.18)} = 8.885$, $p = 0.0036$, Welch's ANOVA; *Rax-CreERT2/+:ArcPomc^loxTB/loxTB* (n = 21) *vs* ArcPomc^loxTB/loxTB (n = 7): $p = 0.0114$; *Rax-CreERT2/+*(n = 6) *vs* ArcPomc^loxTB/loxTB: $p = 0.0139$, Dunnett's T3 multiple comparisons. The mean values for each genotype are shown above their respective columns. **(I)** Bodyweight gain in *Rax-CreERT2/+:ArcPomc^loxTB/loxTB* mice (cohorts 1—6) showed significant inverse correlation with the number of observed *Pomc* neurons in females (red line; $r = -0.75$, $p = 0.0123$, two-tailed, n = 10) but not in males (blue line; $r = -0.48$, $p = 0.1352$, two-tailed, n = 11). The correlation was also significant when the sexes were combined (black line; $r = -0.64$; $p = 0.0019$, two-tailed, n = 21). Scale bar: 200 μm **(D1,** for **D1-F5)**. (For interpretation of the references to color in this figure legend, the reader is referred to the Web version of this article.)

results indicate a linear increase in *Pomc* neuron number from the first TAM injection until around 16 days, with no further increase.

To assess how rapidly new *Pomc* neurons develop efferent projections, we examined POMC fiber distribution in four *Rax-CreERT2/+:Arc-Pomc^loxTB/loxTB* mice from the 7-day group. We observed sparse to modest fiber densities in the BNST, POA, PVH, DMH (Figure 8D—G), along with the thalamic paraventricular and medial amygdaloid nuclei (data not shown), comparable to the low-tier POMC fiber densities

observed 16 weeks after TAM treatment, suggesting the rapid development of fibers from new *Pomc* neurons.

3.7. Congenital Arc *Pomc* deficiency does not significantly affect the rate of *Pomc* neurogenesis from *Rax*⁺ progenitors

Finally, we aimed to determine whether the observed number of newly generated *Pomc* neurons in *Rax-CreERT2/+:ArcPomc^loxTB/loxTB* mice represents normal levels of neurogenesis that also occurs in WT mice,
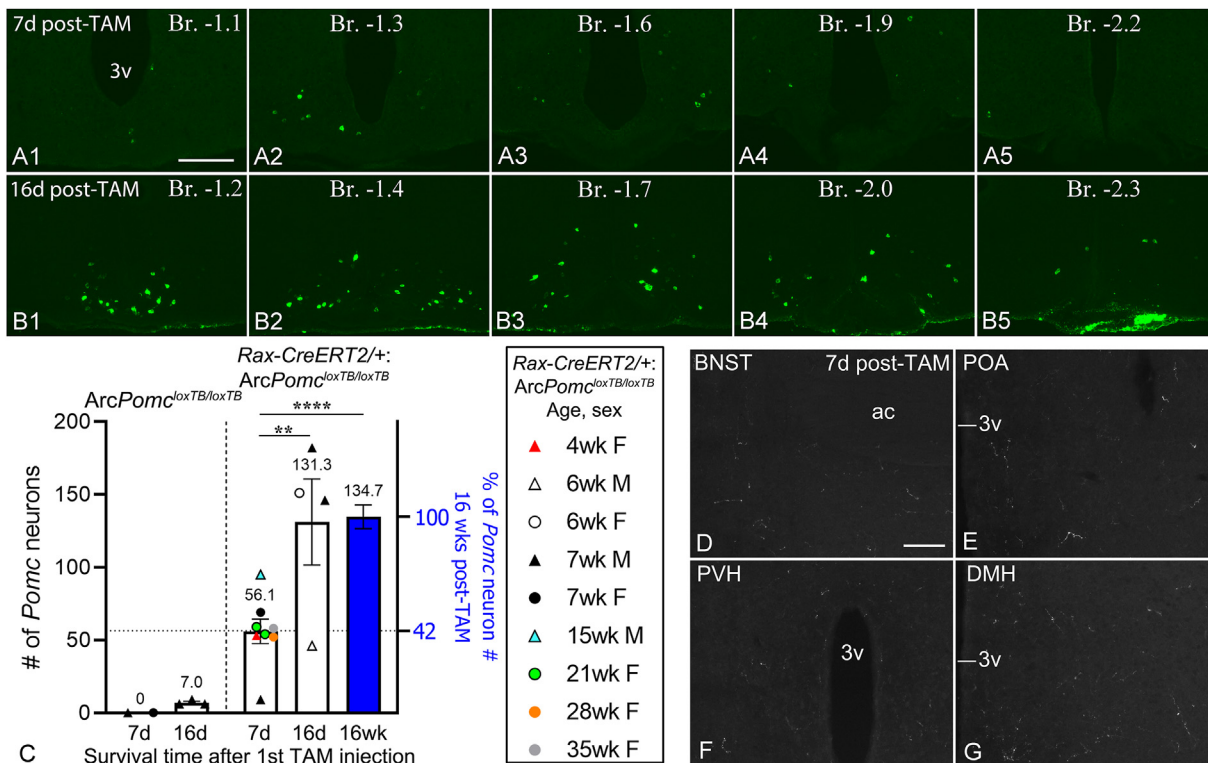
Figure 8: Rapid generation of *Pomc* neurons from *Rax*⁺ progenitors. (A1-B5) FISH detection of hypothalamic *Pomc* neurons in *Rax-CreERT2/+*:Arc*Pomc*^loxTB/loxTB^ mice that were euthanized 7 days **(A1-5)** or 16 days **(B1-5)** after the first TAM injection. The two brains shown here are that of the 35 weeks and 6 weeks old females (refer graph in **C**). Brains from the 7 day-group and 16 week-group were PFA-perfused, while brains from the 16 day-group were collected fresh-frozen. **(C)** *Pomc* neuron counts in *Rax-CreERT2/+*:Arc*Pomc*^loxTB/loxTB^ mice from the 7 day-group (n = 8) and 16 day-group (n = 4). Sex and age (when TAM treatment began) are shown for each mouse in the boxed panel. The blue column represents the *Pomc* neuron count 16 weeks after TAM treatment, combined from both sexes from Figure 3E. $F_{(2,23)} = 14.57$, $p < 0.0001$, one-way ANOVA; ****$p < 0.0001$, **$p = 0.004$, Tukey's multiple comparisons. Arc*Pomc*^loxTB/loxTB^ mice (negative control) were 7-week-old males (triangles) and 13 weeks old females (circle). **(D–G)** POMC fibers (IF) in a *Rax-CreERT2/+*:Arc*Pomc*^loxTB/loxTB^ mouse (7 weeks female) perfused 7 days after TAM treatment began. BNST, bed nucleus of the stria terminalis; POA, preoptic area; PVH, hypothalamic paraventricular nucleus; DMH, hypothalamic dorsomedial nucleus; 3v, third ventricle; ac, anterior commissure. Scale bars: 200 μm **(A1, for A1-B5)**, 100 μm **(D, for D-G)**. (For interpretation of the references to color in this figure legend, the reader is referred to the Web version of this article.)

or rather the result of congenital Arc *Pomc* deficiency itself and/or its metabolic effects. Therefore, we performed lineage tracing using the *Ai34D* reporter allele, *synaptophysin-tdTomato*, to compare *Pomc* neurogenesis in Arc*Pomc*^loxTB/loxTB^ mice with mice expressing the WT *Pomc* alleles. Compound *Rax-CreERT2/+*:Arc*Pomc*^loxTB/loxTB^:*Ai34D* and *Rax-CreERT2/+*:*Ai34D* mice were TAM-treated and euthanized either 16 weeks later as part of the metabolic experiment in early adult mice, or at 7 days as part of the short-term survival experiment. As described above, TAM treatment of these mice results in synaptophysin-tdTomato expression in *Rax*⁺ cells and their progeny. Following *Pomc* FISH, sections were processed for tdTomato IF, and *Pomc* neurons containing the synaptophysin-tdTomato lineage trace were counted (Supplementary Fig 5A1-C3). The numbers of dual-labeled tdTom/*Pomc* neurons were very similar in the two genotypes (Supplementary Fig. 5D), suggesting that Arc *Pomc* deficiency does not significantly affect the rate of *Pomc* neurogenesis from *Rax*⁺ progenitors.

Surprisingly, not all *Pomc* neurons in *Rax-CreERT2/+*:Arc*Pomc*^loxTB/loxTB^:*Ai34D* mice contained synaptophysin-tdTomato (Supplementary Fig 5A1-A2) — the theoretically expected result because both the rescue of *Pomc* transcription and activation of *synaptophysin-tdTomato* expression are CreERT2-dependent. Only a small fraction of *Pomc* neurons, approximately 15–20% was tdTomato positive, in both the 7-day and 16-week groups (Supplementary Fig. 5E). Using an

alternative detection method in the 16-week group, native tdTomato fluorescence was detected in similarly low percentages of immuno-fluorescently labeled POMC neurons (Supplementary Fig. 5E) and corresponding proportions of POMC fibers. Possible explanations for this discrepancy are presented in the Discussion. Notably, the two mice homozygous for the *synaptophysin-tdTomato* allele had both the highest number and percentage of tdTom/*Pomc* neurons (red triangles in Supplementary Fig. 5D and E). It should also be noted that synaptophysin-tdTomato expression itself did not affect *Pomc* neurogenesis from *Rax*⁺ progenitors, as *Pomc* neuron numbers were similar in *Rax-CreERT2/+*:Arc*Pomc*^loxTB/loxTB^:*Ai34D* and *Rax-CreERT2/+*:Arc*Pomc*^loxTB/loxTB^ mice (Supplementary Fig. 5F).

4. DISCUSSION

In this study, we demonstrated that *Rax*⁺ progenitor cells generate a functionally significant population of *Pomc* neurons in adult mice that are capable of mitigating the metabolic abnormalities resulting from congenital Arc *Pomc*-deficiency.

4.1. Validity of the findings

The reliability of genetic fate mapping based on Cre-mediated recombination depends on the specific expression of Cre in the targeted stem/progenitor cell population. In *Rax-CreERT2/+* mice,

CreERT2 was inserted into the *Rax* locus and is expressed under the endogenous *Rax* promoter, thus minimizing, if not eliminating, the possibility of ectopic expression [17]. We did not observe *Rax* expression in hypothalamic neurons by FISH or IF, and *Rax* transcript was not detected in *Pomc* neurons of adult mice in a single-cell RNA-Seq study [35]. Moreover, in a developmental single-cell RNA-Seq analysis of hypothalamic POMC neurons from the Low lab (submitted, [36]), we found that not more than 2% of 3,533 *Pomc*-positive neurons at postnatal age 12 days had any detectable UMIs for *Rax* transcripts (mostly 1—2) compared to typical *Pomc* UMI counts of 50—300 per neuron. As recombination efficiency depends on CreERT2 expression levels [37] and because incomplete recombination occurs even when the CreERT2 driver gene is easily detectable [38,39], these data suggest that it is unlikely for TAM treatment to reactivate *Pomc* expression in already existing Arc neurons. Consequently, the vast majority of Arc *Pomc* neurons observed in *Rax-CreERT2/+*:Arc*Pomc*$^{loxTB/loxTB}$ mice were generated from *Rax*-expressing precursors after TAM induction. Considering that *Pomc* expression in the pituitary and NTS remain intact in Arc*Pomc*$^{loxTB/loxTB}$ mice [21], and there is no evidence of *Rax* expression in the brainstem [17] where the only other POMC neuron population is located [22], the observed metabolic changes can only be attributed to the newly generated Arc *Pomc* neurons.

4.2. Adult-born POMC neurons may derive from two different Rax$^+$ precursors

Although previous studies identified *Rax* as a tanycyte marker [18—20], we found that *Rax* is also expressed in a small population of parenchymal cells. While a subset of these cells had tanycyte-like morphology and probably represents tanycytes that migrated into the parenchyma before differentiation [31,40], the majority represented a different cell type that we termed "frizzy cells", which were located primarily in the caudal Arc. *Rax*-negative frizzy cells expressing tdTomato were more broadly distributed, suggesting that frizzy cells move over long distances and downregulate *Rax* while migrating. Frizzy cells were also observed by other studies, such as by Yoo and colleagues [16] who used the same *Rax-CreERT2/+* line, and showed a reporter-positive cell with glial cell-like morphology that is identical to a frizzy cell. Another tanycyte lineage-tracing study using *Fgf10-CreERT2*$^{/+}$ mice described reporter-positive glial-like cells [40] that are morphologically identical to frizzy cells. A third study using *GLAST::CreERT2* mice to fate map α-tanycytes noted that a large portion of parenchymal reporter-expressing cells was morphologically distinct, unidentified cells, negative for glial markers such as GFAP, nestin, and NG2 [15]. This description resembles frizzy cells, although based on the photographs we could not unambiguously identify them as such. The above studies referred to these cells as having glial morphology or morphologically distinct, confirming that it is difficult to categorize frizzy cells into any known hypothalamic cell type based on morphology. However, frizzy cells may represent a subtype of protoplasmic astrocytes with low GFAP expression/immunoreactivity [30,41], and potentially with neural progenitor characteristics akin to a subtype of hippocampal astrocytes [42]. In a recent RNA-Seq study that categorized cells of the *Rax* lineage, frizzy cells were probably classified as astrocytes and/or oligodendrocyte precursor cells, and it was noted that astrocytes appear to arise directly from α1 and α2 tanycytes [16]. Interestingly, we observed that dorsal α1 tanycytes translocated into the parenchyma with nearby RAX$^+$ frizzy cells (Figure 2B2 inset), which may offer a snapshot into the process of tanycytes entering the parenchyma and differentiating into frizzy cells. Overall, frizzy cells appear to be tanycyte-derived, undifferentiated cells. Further studies are required to investigate whether they are the direct precursors of *Rax*$^+$ progenitor-derived *Pomc* neurons in the lateral Arc; considering their anatomical distribution and the absence of tanycyte-like cells >200 μm away from the third ventricle.

4.3. Dynamics of adult POMC neurogenesis

We found that the number of *Rax*$^+$ progenitor-derived *Pomc* neurons increased linearly up to 16 days after TAM treatment, with no further accumulation. This suggests that *Pomc* neurons are constantly born from *Rax*$^+$ progenitors, have an average lifespan of about 16 days, and undergo turnover. Of note, the population of tdTomato-labeled neurons in *Ai34D* mice increased in a similarly moderate degree between 7 days and 4 months after TAM treatment, further suggesting that *Rax*$^+$ progenitor-derived neurons do not permanently integrate into the brain. Previous studies have suggested a high neuronal turnover rate among both prenatally generated and adult-born hypothalamic neurons, including *Pomc* neurons [9,10]. *Pomc* neurogenesis from *Rax*$^+$ progenitors remained constant up to 15 months of age, in agreement with a previous study on adult hypothalamic neurogenesis [43].

Our observation that *Rax*$^+$ progenitors generated ~10% of the Arc *Pomc* population within 16 days indicates a much more robust *Pomc* neurogenesis than we suspected, based on studies that used BrdU to identify *Pomc* neurons derived from recent cell divisions [8,9]. While this can be partly explained by the superior sensitivity of genetic lineage tracing compared to BrdU labeling, it raises the possibility that the majority of *Rax*$^+$ progenitors might exit the cell cycle several days or weeks before differentiating into *Pomc* neurons. In support, neurogenesis in the Arc from postmitotic precursors without cell division has been reported in adult mice following a monosodium-glutamate—induced lesion [44]. This proposed mechanism raises the question of whether tanycyte proliferation is sufficient to replace the number of postmitotic precursors that exit the ventricular wall and differentiate into neurons. Although basal tanycyte proliferation in mice is modest [15], this question will require careful analysis. In rats, a proliferative zone exists within the α1 tanycyte region [45,46], where proliferation appears to occur in bursts [32]. In addition, tanycyte movement from the β1 to the α domain (ventral to dorsal) was observed in mice [40]. Proliferative activity even among posterior pituitary pituicytes — which also expresses *Rax* [17] and have similar characteristics to tanycytes [47] — could supply new hypothalamic tanycytes by cell migration through the infundibulum. However, proliferation might be insufficient to maintain tanycyte numbers, as age-related attrition in the number of α-tanycytes was described [43].

Using a fluorescent lineage marker, we demonstrated that similar numbers of tdTom/*Pomc* neurons were generated in mice with or without Arc*Pomc*$^{loxTB/loxTB}$ silencing. However, this method dramatically underestimated the number of *Rax*$^+$ progenitor-derived *Pomc* neurons. A possible explanation is that *Rax*$^+$ tanycytes (and frizzy cells) that remained tdTomato-negative in *Rax-CreERT2*:Arc*Pomc*$^{loxTB/loxTB}$:Ai34D mice (Supplementary Fig 6A1-B) generated a significant number of *Pomc* neurons. Cre recombination efficiency depends on the genomic location of the *loxP* sites [37,48], and although we could not determine recombination in the *Pomc* neuronal enhancer at the single-cell level, the *loxP* sites in the *Pomc* gene may be more easily recombined than in the *synaptophysin-tdTomato* allele in the *Rosa26* locus. Nevertheless, as tdTomato-negative *Rax*$^+$ cells represented a small minority of *Rax*$^+$ cells, they may not fully explain why the majority of *Pomc* neurons were tdTomato-negative, unless they over-represented highly active progenitors. Another possibility is that the *synaptophysin-tdTomato* allele may be silenced in differentiated

neurons (refer [49,50] for transgene downregulation following differentiation), as we often observed less intense tdTomato signal in neurons than in tanycytes (examples in Supplementary Fig 5A1-C3). While the exact cause remains to be determined, this provides an important caveat for future lineage tracing studies that rely on similar transgenic alleles.

4.4. Adult-born Pomc neurons become functionally integrated

Our results showed that *Pomc* neurons born from *Rax*$^+$ progenitors develop rapidly and form long-range projections within a week, suggesting fast neuronal maturation, in agreement with findings that adult-born tanycyte-derived neurons become leptin-responsive within 8 days [14]. A recent study also demonstrated that tanycyte-derived neurons are capable of firing action potentials within 12 days, receive synaptic inputs, and thus integrate into the hypothalamic neurocircuitry [16]. Newly generated *Pomc* neurons successfully incorporated into functional neural circuits—as indicated by improved glucose tolerance in males, improved insulin sensitivity, and reduced fat mass that were observed in both sexes, but more pronounced in males. However, food intake and bodyweight did not differ significantly. Interestingly, the opposite effects were observed in studies that interfered with hypothalamic neurogenesis in adult mice. The ablation of tanycytes resulted in modest, but significantly increased fat mass and reduced insulin sensitivity in males only [51]; whereas the inhibition of hypothalamic neurogenesis from *Sox2*-expressing progenitor cells (that also include tanycytes [17]) was accompanied by a ~10% decrease in POMC neuron number, and resulted in glucose intolerance and hyperinsulinemia, but also increased food intake and obesity [8].

It is tempting to speculate that *Rax*$^+$ progenitor-derived *Pomc* neurons primarily regulate glucose homeostasis and energy expenditure, rather than food intake. Recent evidence indicates functional heterogeneity among POMC neurons in the regulation of feeding and energy expenditure [38,52]. For example, rescuing *Pomc* expression in a subset of GABAergic POMC neurons normalized food intake in Arc *Pomc*-deficient mice, while a similar, but nonspecific rescue of *Pomc* expression failed to decrease food intake, though it reduced bodyweight [38]. Alternatively, *Rax*$^+$ progenitor-derived POMC neurons may be involved in food intake regulation, but their number does not reach the threshold to exert a significant effect [38]. Intriguingly, mature adult and middle-aged *Rax-CreERT2*:Arc*Pomc*$^{loxTB/loxTB}$ mice gained significantly less bodyweight than Arc*Pomc*$^{loxTB/loxTB}$ mice following TAM treatment. The weight gain correlated inversely with the number of *Pomc* neurons in females, but was not statistically significant in males. The different metabolic responses observed in males *vs* females occurred despite similar numbers of newly generated *Pomc* neurons in the sexes. Of note, a previous study also found similar levels of neurogenesis in the Arc between males and females [53]. However, female *Rax-CreERT2*:Arc*Pomc*$^{loxTB/loxTB}$ mice consistently exhibited greater densities of POMC fibers than males, which may translate into different metabolic outcomes between the sexes. In addition, distinct POMC neuron subpopulations are known to have disparate effects in males and females. For example, the restoration of *Pomc* expression in Arc*Pomc*$^{loxTB/loxTB}$ mice mediated by a *Htr2c-Cre* knock-in mouse strain normalized the obesity and metabolic phenotype in male offspring [54]. However, females continued to exhibit hypolocomotor activity, decreased energy expenditure, and obesity, despite normalized feeding behavior and insulin levels. Furthermore, chemogenetic activation of leptin-receptor-expressing and glucagon-like peptide 1 receptor-expressing POMC neurons suppresses feeding in male mice, but not in female mice [55].

5. CONCLUSIONS

In conclusion, adult-born *Pomc* neurons generated by *Rax*$^+$ progenitors make up ~10% of the total *Pomc* neuron population and are sufficient to mitigate the metabolic abnormalities of congenital Arc *Pomc*-deficiency, revealing a remarkable novel regulatory capacity of *Pomc* neurons. However, further experiments are required to determine the underlying mechanisms involved in the generation of *Pomc* neurons from *Rax*$^+$ progenitors. Because adult *Pomc* neurogenesis has the potential to slow the progression of advanced obesity caused by Arc *Pomc* deficiency in mice, we propose that developing interventions to increase the number of adult-born *Pomc* neurons in humans may lead to a novel clinical approach in the treatment of diabetes and obesity.

AUTHOR CONTRIBUTIONS

Study concept: RML. Overall research plan and study supervision: MJL and RML. Generation of experimental mice, metabolic experiments, and data analysis: S. Histology and data analysis: GW. Article writing: S and GW. Critical revision of the article: MJL and RML.

ACKNOWLEDGMENTS

CONFLICT OF INTEREST

None declared.

APPENDIX A. SUPPLEMENTARY DATA

Supplementary data to this article can be found online at https://doi.org/10.1016/j.molmet.2021.101312.

REFERENCES

[1] Berthoud, H.R., Munzberg, H., Morrison, C.D., 2017. Blaming the brain for obesity: integration of hedonic and homeostatic mechanisms. Gastroenterology 152(7):1728—1738.

[2] Krashes, M.J., Lowell, B.B., Garfield, A.S., 2016. Melanocortin-4 receptor-regulated energy homeostasis. Nature Neuroscience 19(2):206—219.

[3] Anderson, E.J., Cakir, I., Carrington, S.J., Cone, R.D., Ghamari-Langroudi, M., Gillyard, T., et al., 2016. 60 years OF POMC: regulation of feeding and energy homeostasis by alpha-MSH. Journal of Molecular Endocrinology 56(4):T157—T174.

[4] Smart, J.L., Tolle, V., Low, M.J., 2006. Glucocorticoids exacerbate obesity and insulin resistance in neuron-specific proopiomelanocortin-deficient mice. Journal of Clinical Investigation 116(2):495—505.

[5] Bumaschny, V.F., Yamashita, M., Casas-Cordero, R., Otero-Corchon, V., de Souza, F.S., Rubinstein, M., et al., 2012. Obesity-programmed mice are rescued by early genetic intervention. Journal of Clinical Investigation 122(11): 4203—4212.

6 Chhabra, K.H., Adams, J.M., Jones, G.L., Yamashita, M., Schlapschy, M., Skerra, A., et al., 2016. Reprogramming the bodyweight set point by a

reciprocal interaction of hypothalamic leptin sensitivity and Pomc gene expression reverts extreme obesity. Molecular Metabolism 5(10):869−881.

[7] Yoo, S., Blackshaw, S., 2018. Regulation and function of neurogenesis in the adult mammalian hypothalamus. Progress in Neurobiology 170: 53−66.

[8] Li, J., Tang, Y., Cai, D., 2012. IKKbeta/NF-kappaB disrupts adult hypothalamic neural stem cells to mediate a neurodegenerative mechanism of dietary obesity and pre-diabetes. Nature Cell Biology 14(10):999−1012.

[9] Gouaze, A., Brenachot, X., Rigault, C., Krezymon, A., Rauch, C., Nedelec, E., et al., 2013. Cerebral cell renewal in adult mice controls the onset of obesity. PloS One 8(8):e72029.

[10] McNay, D.E., Briancon, N., Kokoeva, M.V., Maratos-Flier, E., Flier, J.S., 2012. Remodeling of the arcuate nucleus energy-balance circuit is inhibited in obese mice. Journal of Clinical Investigation 122(1):142−152.

[11] Rodriguez, E.M., Blazquez, J.L., Pastor, F.E., Pelaez, B., Pena, P., Peruzzo, B., et al., 2005. Hypothalamic tanycytes: a key component of brain-endocrine interaction. International Review of Cytology 247:89−164.

[12] Xu, Y., Tamamaki, N., Noda, T., Kimura, K., Itokazu, Y., Matsumoto, N., et al., 2005. Neurogenesis in the ependymal layer of the adult rat 3rd ventricle. Experimental Neurology 192(2):251−264.

[13] Lee, D.A., Bedont, J.L., Pak, T., Wang, H., Song, J., Miranda-Angulo, A., et al., 2012. Tanycytes of the hypothalamic median eminence form a diet-responsive neurogenic niche. Nature Neuroscience 15(5):700−702.

[14] Haan, N., Goodman, T., Najdi-Samiei, A., Stratford, C.M., Rice, R., El Agha, E., et al., 2013. Fgf10-expressing tanycytes add new neurons to the appetite/energy-balance regulating centers of the postnatal and adult hypothalamus. Journal of Neuroscience 33(14):6170−6180.

[15] Robins, S.C., Stewart, I., McNay, D.E., Taylor, V., Giachino, C., Goetz, M., et al., 2013. alpha-Tanycytes of the adult hypothalamic third ventricle include distinct populations of FGF-responsive neural progenitors. Nature Communications 4: 2049.

[16] Yoo, S., Kim, J., Lyu, P., Hoang, T.V., Ma, A., Trinh, V., et al., 2021. Control of neurogenic competence in mammalian hypothalamic tanycytes. bioRxiv. https://doi.org/10.1101/2020.11.02.359992.

[17] Pak, T., Yoo, S., Miranda-Angulo, A.L., Wang, H., Blackshaw, S., 2014. Rax-CreERT2 knock-in mice: a tool for selective and conditional gene deletion in progenitor cells and radial glia of the retina and hypothalamus. PloS One 9(4): e90381.

[18] Miranda-Angulo, A.L., Byerly, M.S., Mesa, J., Wang, H., Blackshaw, S., 2014. Rax regulates hypothalamic tanycyte differentiation and barrier function in mice. Journal of Comparative Neurology 522(4):876−899.

[19] Campbell, J.N., Macosko, E.Z., Fenselau, H., Pers, T.H., Lyubetskaya, A., Tenen, D., et al., 2017. A molecular census of arcuate hypothalamus and median eminence cell types. Nature Neuroscience 20(3):484−496.

[20] Chen, R., Wu, X., Jiang, L., Zhang, Y., 2017. Single-cell RNA-seq reveals hypothalamic cell diversity. Cell Reports 18(13):3227−3241.

[21] Lam, D.D., de Souza, F.S., Nasif, S., Yamashita, M., Lopez-Leal, R., Otero-Corchon, V., et al., 2015. Partially redundant enhancers cooperatively maintain Mammalian pomc expression above a critical functional threshold. PLoS Genetics 11(2):e1004935.

[22] Young, J.I., Otero, V., Cerdan, M.G., Falzone, T.L., Chan, E.C., Low, M.J., et al., 1998. Authentic cell-specific and developmentally regulated expression of pro-opiomelanocortin genomic fragments in hypothalamic and hindbrain neurons of transgenic mice. Journal of Neuroscience 18(17):6631−6640.

[23] Jahn, H.M., Kasakow, C.V., Helfer, A., Michely, J., Verkhratsky, A., Maurer, H.H., et al., 2018. Refined protocols of tamoxifen injection for inducible DNA recombination in mouse astroglia. Scientific Reports 8(1): 5913.

[24] Jarvela, T.S., Surbhi, Shakya, M., Bachor, T., White, A., Low, M.J., et al., 2019. Reduced stability and pH-dependent activity of a common obesity-linked PCSK1 polymorphism, N221D. Endocrinology 160(11):2630−2645.

[25] Allison, D.B., Paultre, F., Maggio, C., Mezzitis, N., Pi-Sunyer, F.X., 1995. The use of areas under curves in diabetes research. Diabetes Care 18(2):245−250.

[26] Henriksen, E.J., Jacob, S., Fogt, D.L., Dietze, G.J., 1998. Effect of chronic bradykinin administration on insulin action in an animal model of insulin resistance. American Journal of Physiology 275(1):R40−R45.

[27] Matthews, D.R., Hosker, J.P., Rudenski, A.S., Naylor, B.A., Treacher, D.F., Turner, R.C., 1985. Homeostasis model assessment: insulin resistance and beta-cell function from fasting plasma glucose and insulin concentrations in man. Diabetologia 28(7):412−419.

[28] Wittmann, G., Hrabovszky, E., Lechan, R.M., 2013. Distinct glutamatergic and GABAergic subsets of hypothalamic pro-opiomelanocortin neurons revealed by in situ hybridization in male rats and mice. Journal of Comparative Neurology 521(14):3287−3302.

[29] Salvatierra, J., Lee, D.A., Zibetti, C., Duran-Moreno, M., Yoo, S., Newman, E.A., et al., 2014. The LIM homeodomain factor Lhx2 is required for hypothalamic tanycyte specification and differentiation. Journal of Neuroscience 34(50):16809−16820.

[30] Cardona, S.M., Dunphy, J.M., Das, A.S., Lynch, C.R., Lynch, W.P., 2019. Astrocyte infection is required for retrovirus-induced spongiform neuro-degeneration despite suppressed viral protein expression. Frontiers in Neuroscience 13:1166.

[31] Jourdon, A., Gresset, A., Spassky, N., Charnay, P., Topilko, P., Santos, R., 2016. Prss56, a novel marker of adult neurogenesis in the mouse brain. Brain Structure and Function 221(9):4411−4427.

[32] Wittmann, G., Lechan, R.M., 2018. Prss56 expression in the rodent hypothalamus: inverse correlation with pro-opiomelanocortin suggests oscillatory gene expression in adult rat tanycytes. Journal of Comparative Neurology 526(15):2444−2461.

[33] Lam, D.D., Attard, C.A., Mercer, A.J., Myers Jr., M.G., Rubinstein, M., Low, M.J., 2015. Conditional expression of Pomc in the Lepr-positive sub-population of POMC neurons is sufficient for normal energy homeostasis and metabolism. Endocrinology 156(4):1292−1302.

[34] Flurkey, K., Currer, J., Harrison, D., 2007. The mouse in aging research. In: Fox, J. (Ed.), The mouse in biomedical research, 2nd ed. Academic Press. p. 637−72.

[35] Lam, B.Y.H., Cimino, I., Polex-Wolf, J., Nicole Kohnke, S., Rimmington, D., Iyemere, V., et al., 2017. Heterogeneity of hypothalamic pro-opiomelanocortin-expressing neurons revealed by single-cell RNA sequencing. Molecular Metabolism 6(5):383−392.

[36] Yu, H., Rubinstein, M., Low, M.J., 2021. Dual origin and multiple neuro-peptidergic trajectories of hypothalamic POMC progenitors revealed by developmental single-cell transcriptomics. bioRxiv. https://doi.org/10.1101/2021.05.12.443898.

[37] Fernandez-Chacon, M., Casquero-Garcia, V., Luo, W., Francesca Lunella, F., Ferreira Rocha, S., Del Olmo-Cabrera, S., et al., 2019. iSuRe-Cre is a genetic tool to reliably induce and report Cre-dependent genetic modifications. Nature Communications 10(1):2262.

[38] Trotta, M., Bello, E.P., Alsina, R., Tavella, M.B., Ferran, J.L., Rubinstein, M., et al., 2020. Hypothalamic Pomc expression restricted to GABAergic neurons suppresses Npy overexpression and restores food intake in obese mice. Molecular Metabolism 37:100985.

[39] Jarvie, B.C., Hentges, S.T., 2012. Expression of GABAergic and glutamatergic phenotypic markers in hypothalamic proopiomelanocortin neurons. Journal of Comparative Neurology 520(17):3863−3876.

[40] Goodman, T., Nayar, S.G., Clare, S., Mikolajczak, M., Rice, R., Mansour, S., et al., 2020. Fibroblast growth factor 10 is a negative regulator of postnatal neurogenesis in the mouse hypothalamus. Development 147(13).

[41] DeSilva, T.M., Borenstein, N.S., Volpe, J.J., Kinney, H.C., Rosenberg, P.A., 2012. Expression of EAAT2 in neurons and protoplasmic astrocytes during human cortical development. Journal of Comparative Neurology 520(17):3912—3932.

[42] Batiuk, M.Y., Martirosyan, A., Wahis, J., de Vin, F., Marneffe, C., Kusserow, C., et al., 2020. Identification of region-specific astrocyte subtypes at single cell resolution. Nature Communications 11(1):1220.

[43] Chaker, Z., George, C., Petrovska, M., Caron, J.B., Lacube, P., Caille, I., et al., 2016. Hypothalamic neurogenesis persists in the aging brain and is controlled by energy-sensing IGF-I pathway. Neurobiology of Aging 41:64—72.

[44] Yulyaningsih, E., Rudenko, I.A., Valdearcos, M., Dahlen, E., Vagena, E., Chan, A., et al., 2017. Acute lesioning and rapid repair of hypothalamic neurons outside the blood-brain barrier. Cell Reports 19(11):2257—2271.

[45] Perez-Martin, M., Cifuentes, M., Grondona, J.M., Lopez-Avalos, M.D., Gomez-Pinedo, U., Garcia-Verdugo, J.M., et al., 2010. IGF-I stimulates neurogenesis in the hypothalamus of adult rats. European Journal of Neuroscience 31(9):1533—1548.

[46] Recabal, A., Fernandez, P., Lopez, S., Barahona, M.J., Ordenes, P., Palma, A., et al., 2020. The FGF2-induced tanycyte proliferation involves a connexin 43 hemichannel/purinergic-dependent pathway. Journal of Neurochemistry.

[47] Rodriguez, E., Guerra, M., Peruzzo, B., Blazquez, J.L., 2019. Tanycytes: a rich morphological history to underpin future molecular and physiological investigations. Journal of Neuroendocrinology 31(3):e12690.

[48] Vooijs, M., Jonkers, J., Berns, A., 2001. A highly efficient ligand-regulated Cre recombinase mouse line shows that LoxP recombination is position dependent. EMBO Reports 2(4):292—297.

[49] Jakobsson, J., Rosenqvist, N., Thompson, L., Barraud, P., Lundberg, C., 2004. Dynamics of transgene expression in a neural stem cell line transduced with lentiviral vectors incorporating the cHS4 insulator. Experimental Cell Research 298(2):611—623.

[50] Macarthur, C.C., Xue, H., Van Hoof, D., Lieu, P.T., Dudas, M., Fontes, A., et al., 2012. Chromatin insulator elements block transgene silencing in engineered human embryonic stem cell lines at a defined chromosome 13 locus. Stem Cells and Development 21(2):191—205.

[51] Yoo, S., Cha, D., Kim, S., Jiang, L., Cooke, P., Adebesin, M., et al., 2020. Tanycyte ablation in the arcuate nucleus and median eminence increases obesity susceptibility by increasing body fat content in male mice. Glia 68(10):1987—2000.

[52] Saucisse, N., Mazier, W., Simon, V., Binder, E., Catania, C., Bellocchio, L., et al., 2020. POMC neurons functional heterogeneity relies on mTORC1 signaling. bioRxiv. https://doi.org/10.1101/2020.03.25.007765.

[53] Lee, D.A., Yoo, S., Pak, T., Salvatierra, J., Velarde, E., Aja, S., et al., 2014. Dietary and sex-specific factors regulate hypothalamic neurogenesis in young adult mice. Frontiers in Neuroscience 8:157.

[54] Burke, L.K., Doslikova, B., D'Agostino, G., Greenwald-Yarnell, M., Georgescu, T., Chianese, R., et al., 2016. Sex difference in physical activity, energy expenditure and obesity driven by a subpopulation of hypothalamic POMC neurons. Molecular Metabolism 5(3):245—252.

[55] Biglari, N., Gaziano, I., Schumacher, J., Radermacher, J., Paeger, L., Klemm, P., et al., 2021. Functionally distinct POMC-expressing neuron subpopulations in hypothalamus revealed by intersectional targeting. Nature Neuroscience.